Electromagnetic Nondestructive Evaluation (ENDE)
Workshop 2009
July 21-23, 2009; Dayton, Ohio

Multivariate Inverse Methods for Magnetoquasistatic and Electroquasistatic NDE

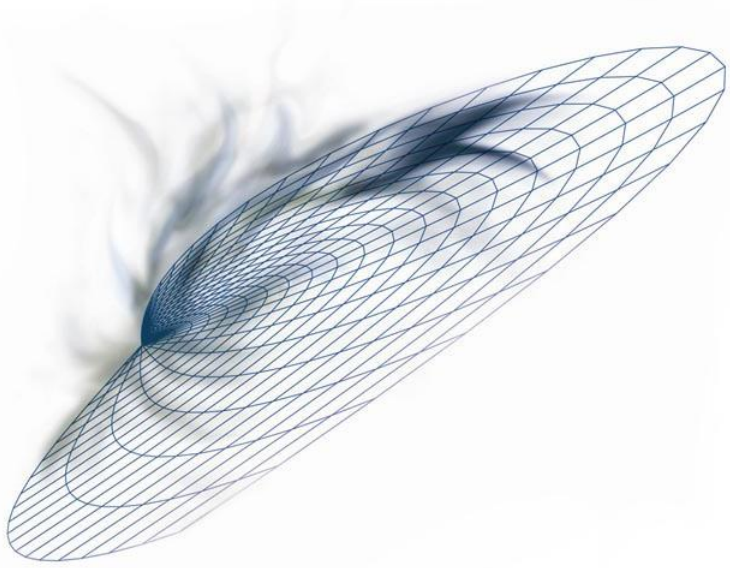

Dr. Neil Goldfine and Dr. Yanko Sheiretov

JENTEK Sensors, Inc.,
110-1 Clematis Avenue, Waltham, MA
Phone: 781-642-9666
Email: jentek@shore.net

© JENTEK Sensors 2009

History & Acknowledgements

Professor James R. Melcher 1970's and 80's


Dr. Neil Goldfine
Dr. Andrew Washabaugh 1980's through 2009


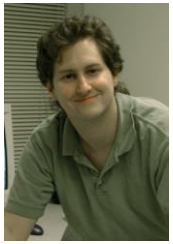

Dr. Yanko Sheiretov 1990's through 2009
Dr. Darrell Schlicker

For research at MIT LEES, initially under the late Prof. James Melcher and more recently under Prof. Marcus Zahn, and continued at JENTEK Sensors, Inc.

© JENTEK Sensors 2009

History & Acknowledgements (continued)

We would like to acknowledge funding from the US Air Force and the US Navy in particular, as well as other agencies, including, Army, NASA, DOE, DOT and DARPA.

We believe we have delivered a substantial return on investment for this government funding

© JENTEK Sensors 2009

A Two Part Presentation

Dr. Neil Goldfine

Introduction to

- Design, Calibration, Measurement, Inverse Methods, Filters, Decisions
- MWM and MWM-Array Sensors & IDED and IDED-Array Sensors
- Applications (cracks, coatings, corrosion, stress, temperature)
  - Grids and Lattices for Multivariate Inverse Methods
  - Air and Reference Calibration
  - Signature Libraries & Time-Sequenced Imaging for Enhanced Detection

Motivation & Applications

Dr. Yanko Sheiretov

Background on

- Sensor Model
  - Two-port Impedance Matrices, Transimpedance, Maxwell's Equations, Quasistatic Regimes, EM-field Partial Differential Equations and Solutions
- Multivariate Inverse Methods
  - Searching in multi-dimensional nonlinear spaces
  - Multi-dimensional nonlinear interpolation

Physics & Details

© JENTEK Sensors 2009

Steps to Solving Challenging NDE Problems

- Sensor Design
- Calibration *(Standardization)*
- Measurement/Data Acquisition
- Multivariate Inverse Method
- Filters
- Decision Support Software

© JENTEK Sensors 2009

MWM® & MWM-Array Eddy Current Sensors

Single-channel
MWM sensor FS35

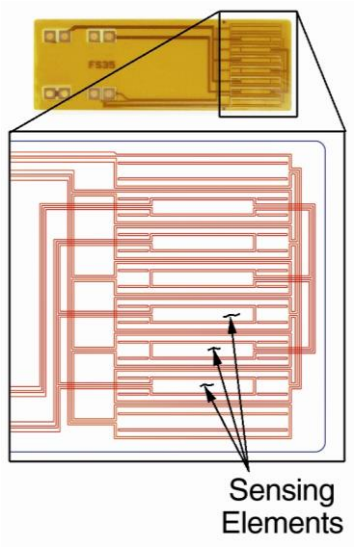

Multiple channel
MWM-Array sensor FA28

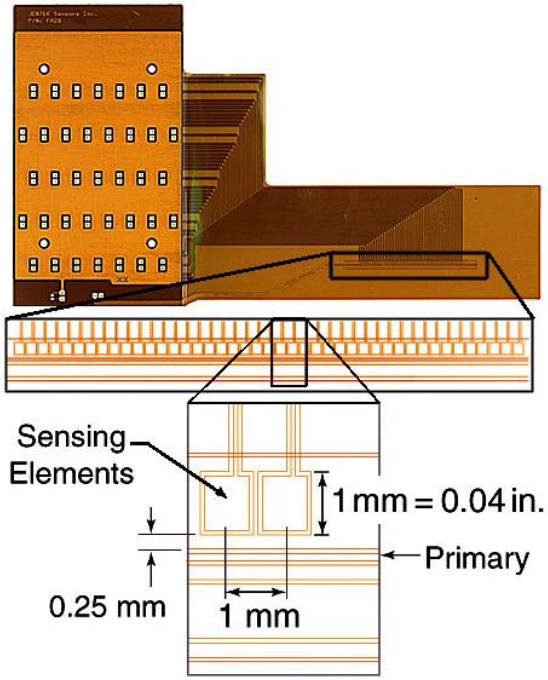

Paradigm Shift

Design Sensors with rapid and accurate modeling as the primary focus

Multiple channel
MWM-Array FA106

© JENTEK Sensors 2009

Air, Shunt Calibration (No Crack Standards) Now a U.S. Navy and Air Force Standard Practice

Sensor in "air"

Shunt Tip

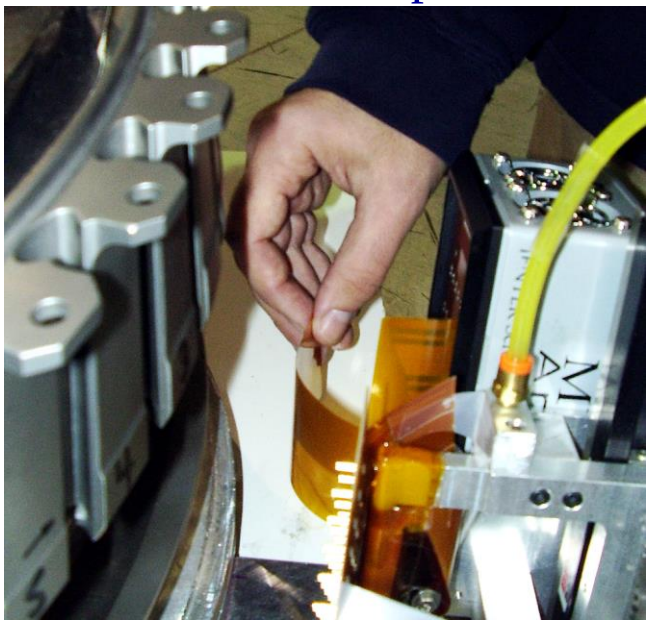

Easy to Replace Cartridges:

- Sensor
- Shuttle
- Balloons

© JENTEK Sensors 2009

1993 Materials Evaluation Paper, Goldfine (Melcher)

Multivariate Inverse Method using Pre-computed Measurement Grids

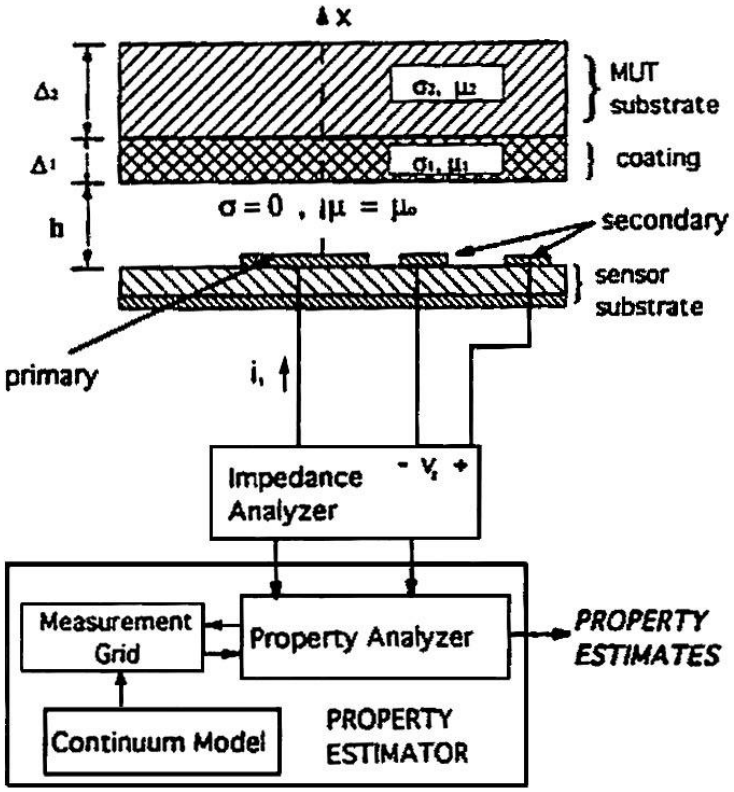

Figure 5—MWM prototype measurement system.

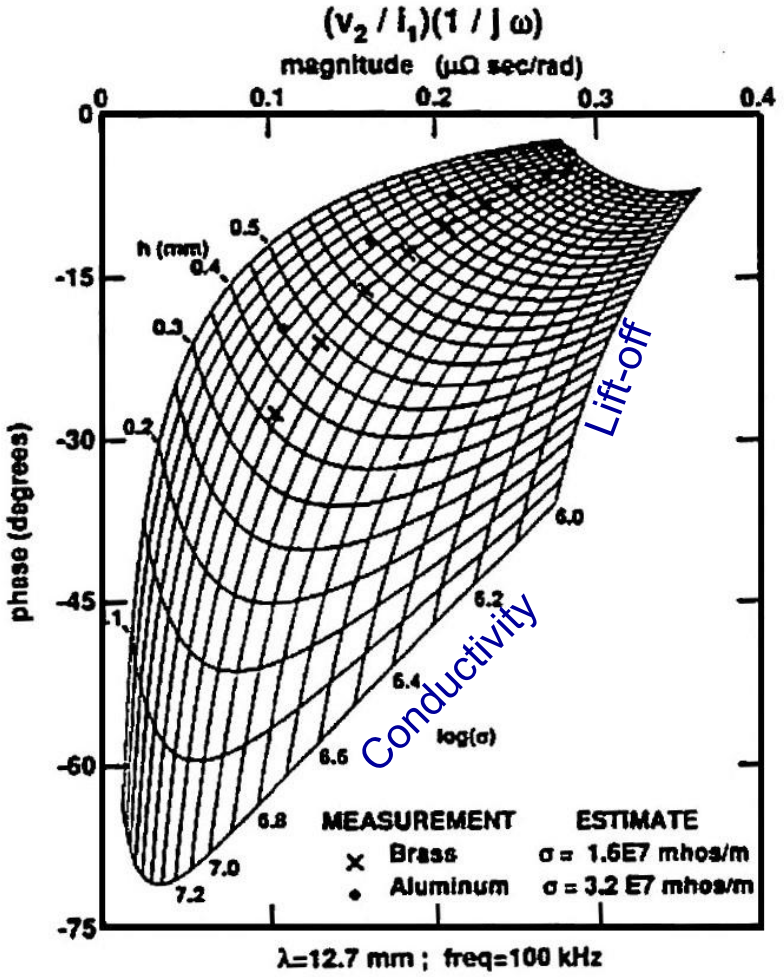

Figure 6—Property estimation grid for independent conductivity, σ, and liftoff, h, measurement (λ = 12.7 mm, f = 158 KHz).

Published, *Materials Evaluation* 1993

© JENTEK Sensors 2009

1993 Materials Evaluation Paper, Goldfine (Melcher)

Singular Value Decomposition for Measurement Procedure Development and Sensor Design

$$d\vec{\Gamma} = J\,d\theta$$

$$d\vec{\Gamma}_r = \frac{\partial \vec{\Gamma}_r}{\partial \sigma} d\sigma + \frac{\partial \vec{\Gamma}_r}{\partial \Delta} d\Delta$$

$$d\vec{\Gamma}_i = \frac{\partial \vec{\Gamma}_i}{\partial \sigma} d\sigma + \frac{\partial \vec{\Gamma}_i}{\partial \Delta} d\Delta$$

$$d\vec{\Gamma} = \begin{bmatrix} d\vec{\Gamma}_r \\ d\vec{\Gamma}_i \end{bmatrix}$$

$$d\theta = \begin{bmatrix} d\sigma \\ d\Delta \end{bmatrix}$$

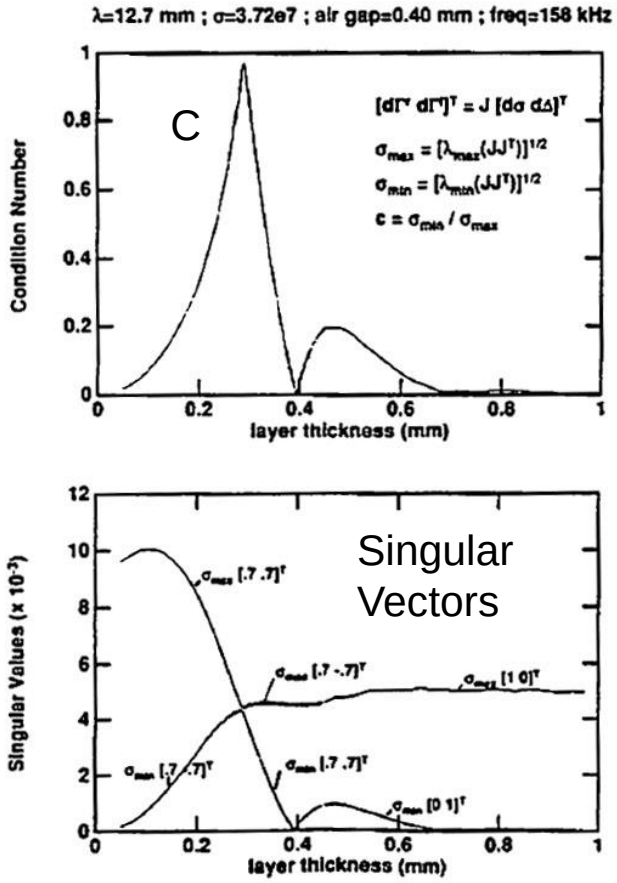

$$[d\Gamma^r\ d\Gamma^i]^T = J\,[d\sigma\ d\Delta]^T$$

$$\sigma_{max} = [\lambda_{max}(JJ^T)]^{1/2}$$

$$\sigma_{min} = [\lambda_{min}(JJ^T)]^{1/2}$$

$$c = \sigma_{min} / \sigma_{max}$$

= Condition Number

= ratio of min/max singular values

Figure 10—Condition number C, maximum and minimum singular values, σ_{max}, σ_{min}, and right-singular vectors of the Jacobian, J, as a function of the coating thickness, Δ, for an aluminum coating on an insulating substrate.

Materials Evaluation 1993

© JENTEK Sensors 2009

1993 Materials Evaluation Paper, Goldfine (Melcher)

Singular Value Decomposition for Measurement Procedure Development and Sensor Design

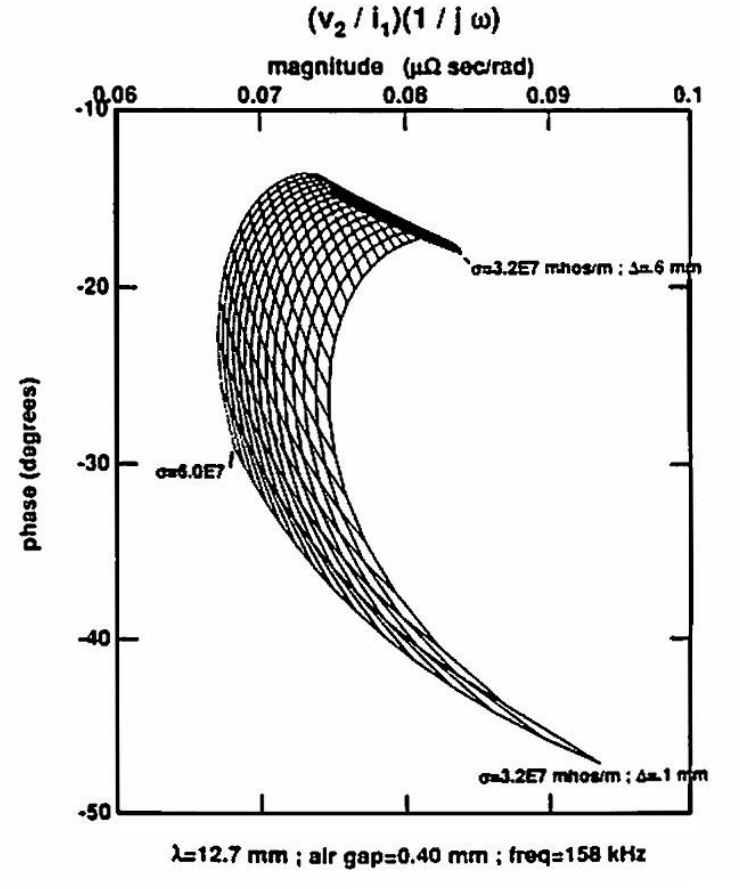

Figure 9—Property estimation grid for independent coating conductivity, σ, and thickness, Δ, measurement (λ = 12.7 mm, f = 158 KHz, h = 0.4 mm), for a metal coating on an insulating substrate.

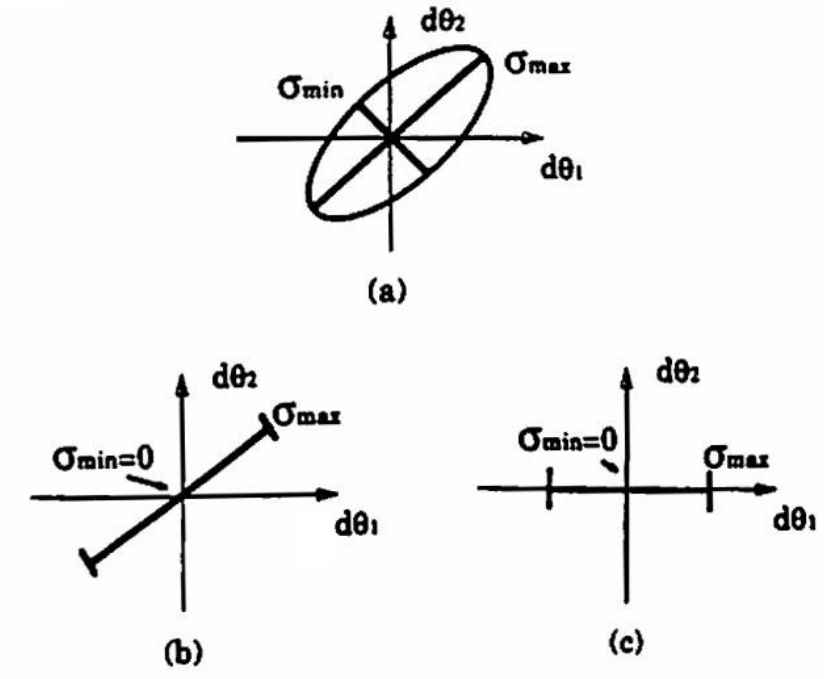

Figure 8—Generalized sensitivity ellipsoids for singular-value decomposition on a 2 by 2 Jacobian with unknown vector $[d\theta_1\ d\theta_2]^T$: (a) example of good selectivity, (b) unobservable mode $[0.7\ -0.7]^T$, and (c) unobservable mode $[0\ 1]^T$.

© JENTEK Sensors 2009

1993 Materials Evaluation Paper, Goldfine (Melcher)

Singular Value Decomposition for Measurement Procedure Development and Sensor Design

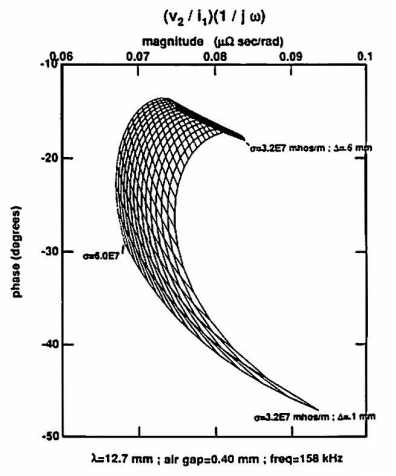

Figure 9—Property estimation grid for independent coating conductivity, σ, and thickness, Δ, measurement (λ = 12.7 mm, f = 158 KHz, h = 0.4 mm), for a metal coating on an insulating substrate.

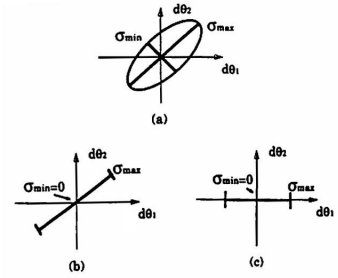

Figure 8—Generalized sensitivity ellipsoids for singular-value decomposition on a 2 by 2 Jacobian with unknown vector $[d\theta_1\ d\theta_2]^T$: (a) example of good selectivity, (b) unobservable mode $[0.7\ -0.7]^T$, and (c) unobservable mode $[0\ 1]^T$.

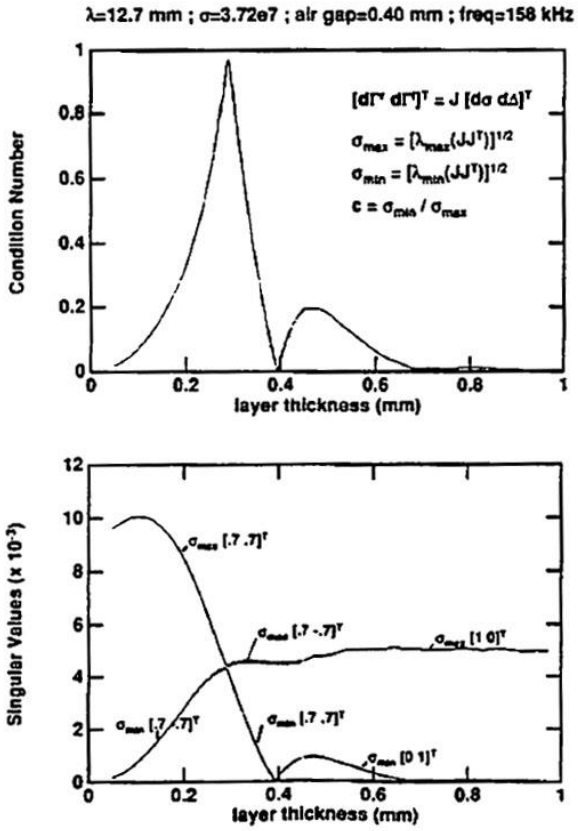

Figure 10—Condition number C, maximum and minimum singular values, σ_{max}, σ_{min}, and right-singular vectors of the Jacobian, J, as a function of the coating thickness, Δ, for an aluminum coating on an insulating substrate.

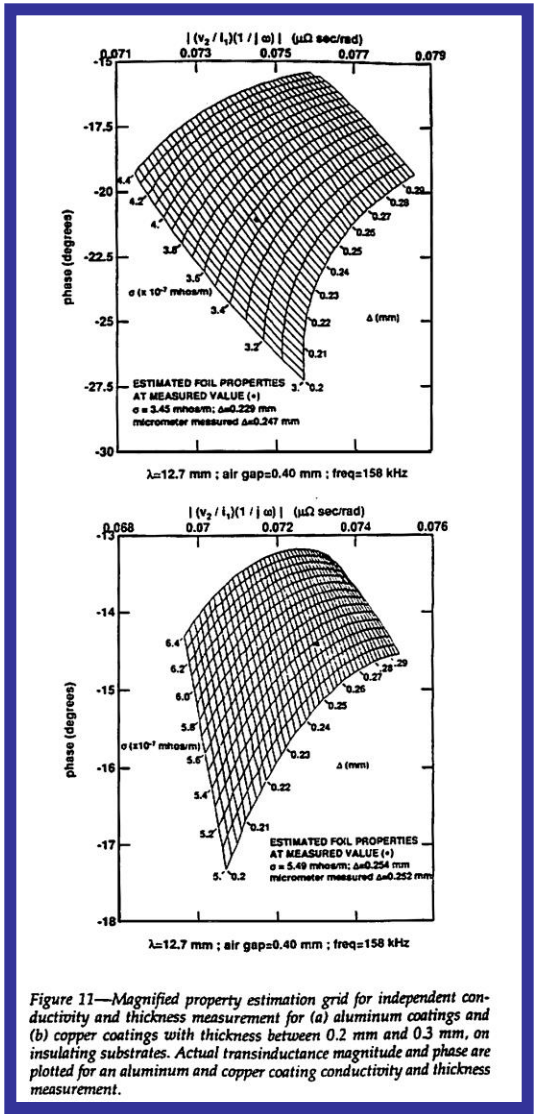

Figure 11—Magnified property estimation grid for independent conductivity and thickness measurement for (a) aluminum coatings and (b) copper coatings with thickness between 0.2 mm and 0.3 mm, on insulating substrates. Actual transinductance magnitude and phase are plotted for an aluminum and copper coating conductivity and thickness measurement.

© JENTEK Sensors 2009

Depth of Penetration for MWM Sensors and MWM-Arrays

Field Variation with Depth $\sim e^{-\Gamma_n z}$

Spatial Fourier Mode Depth of Penetration = $1/\Re e(\Gamma_n)$

$$\Gamma_n = \sqrt{(2\pi n/\lambda)^2 + 2j/\delta^2}$$

Skin depth: $\delta = \sqrt{1/(\pi f \mu \sigma)}$

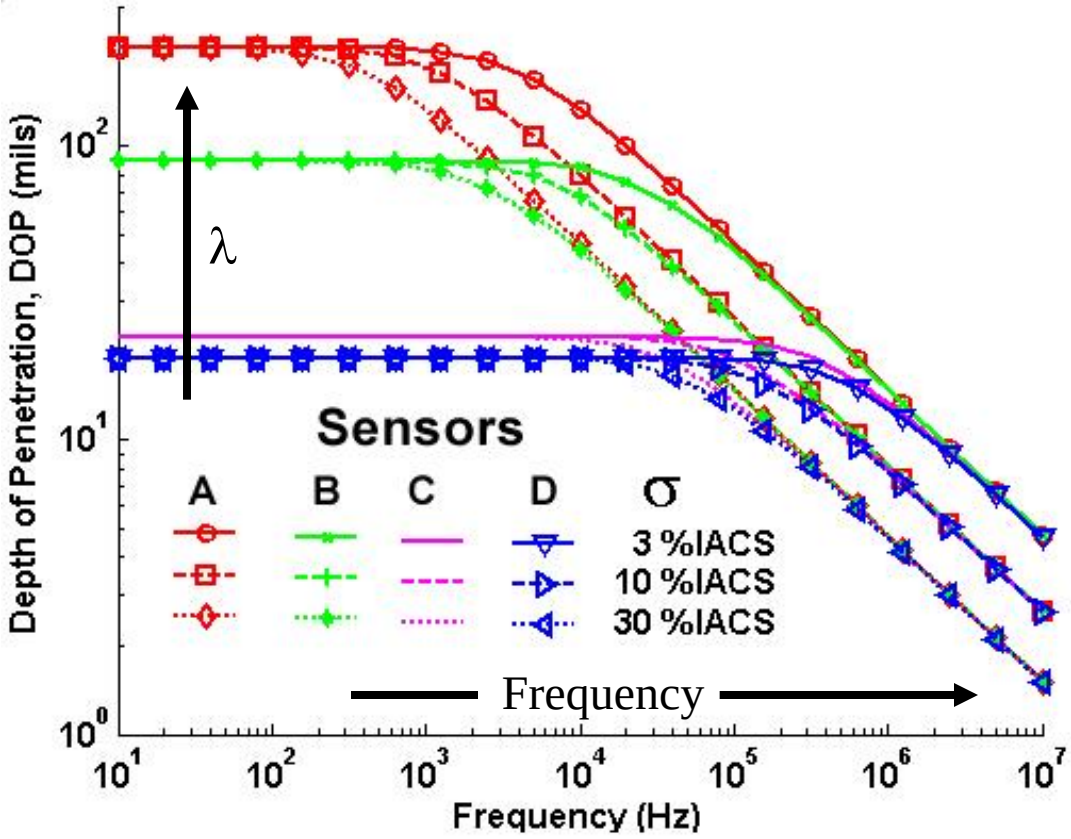

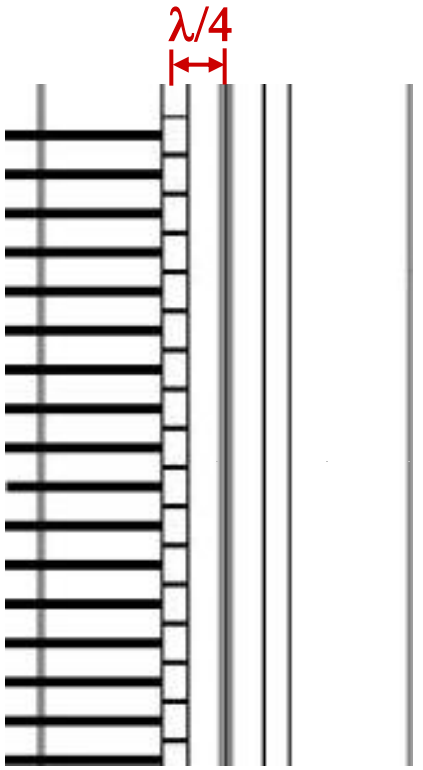

© JENTEK Sensors 2009

Interdigitated Electrode (IDED®) Dielectrometer

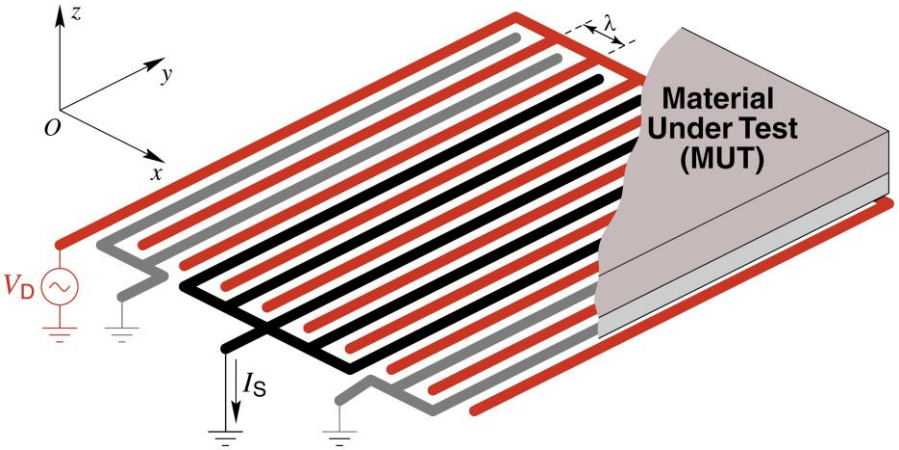

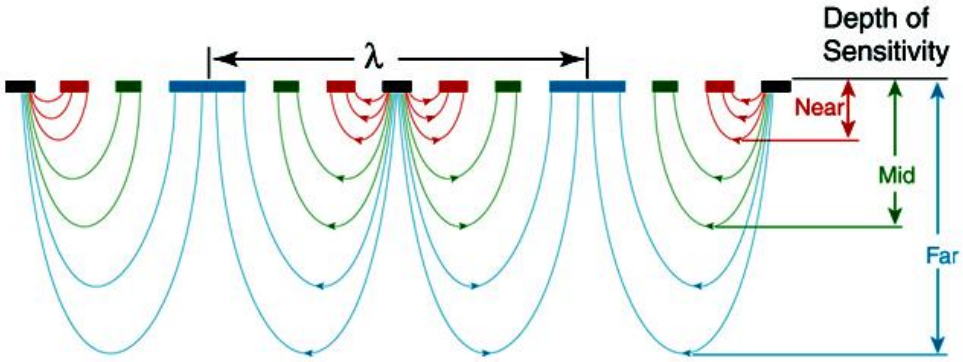

Three-wavelength co-located segmented-field dielectrometer

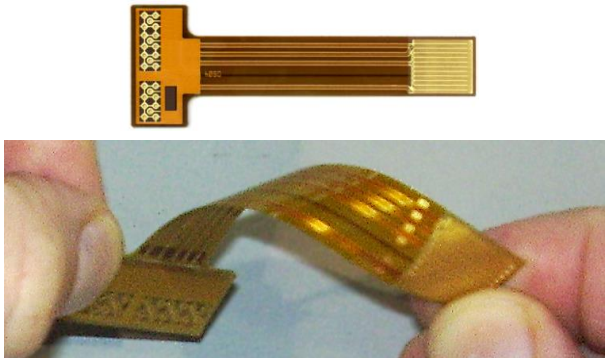

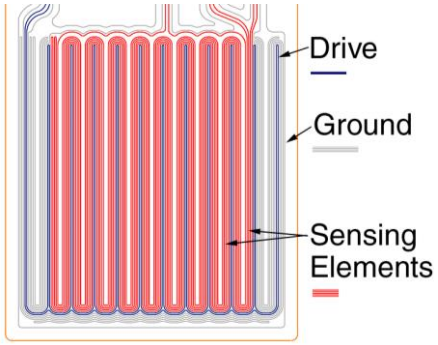

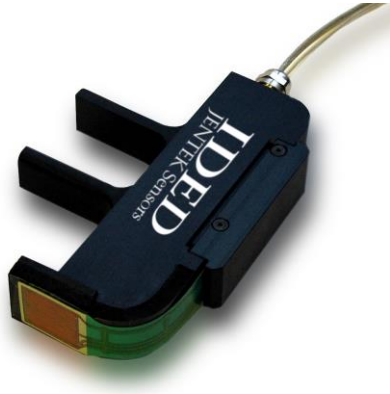

© JENTEK Sensors 2009

Example Applications

- Conductivity Imaging for Cracks and Residual Stresses
- Coating Characterization
- Non-Contact Torque, Axial and Bending loads

© JENTEK Sensors 2009

MWM-Array Conductivity Imaging History

% Absolute Conductivity Change*

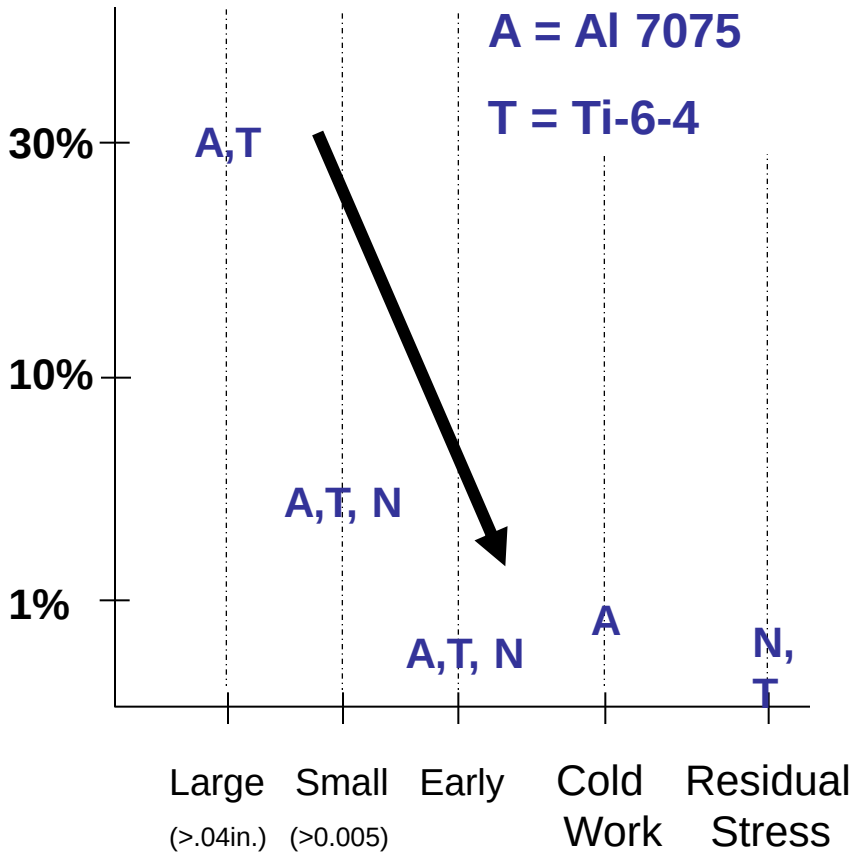

Application	MWM-Array Measured Conductivity Change*	
	Al	Ti Ni
"Large Cracks" **Length > 0.03in.**	> 8%	>8%
"Small" Cracks **Length >0.005 in.**	1-8%	1-8%
Early Fatigue (micro-cracks)	<1%	<1%
Cold work	~1%	N/A
Residual Stress	N/A	<0.3%, <1%

© JENTEK Sensors 2009

Rapid Data Processing with Grid Methods and "Air" Calibration

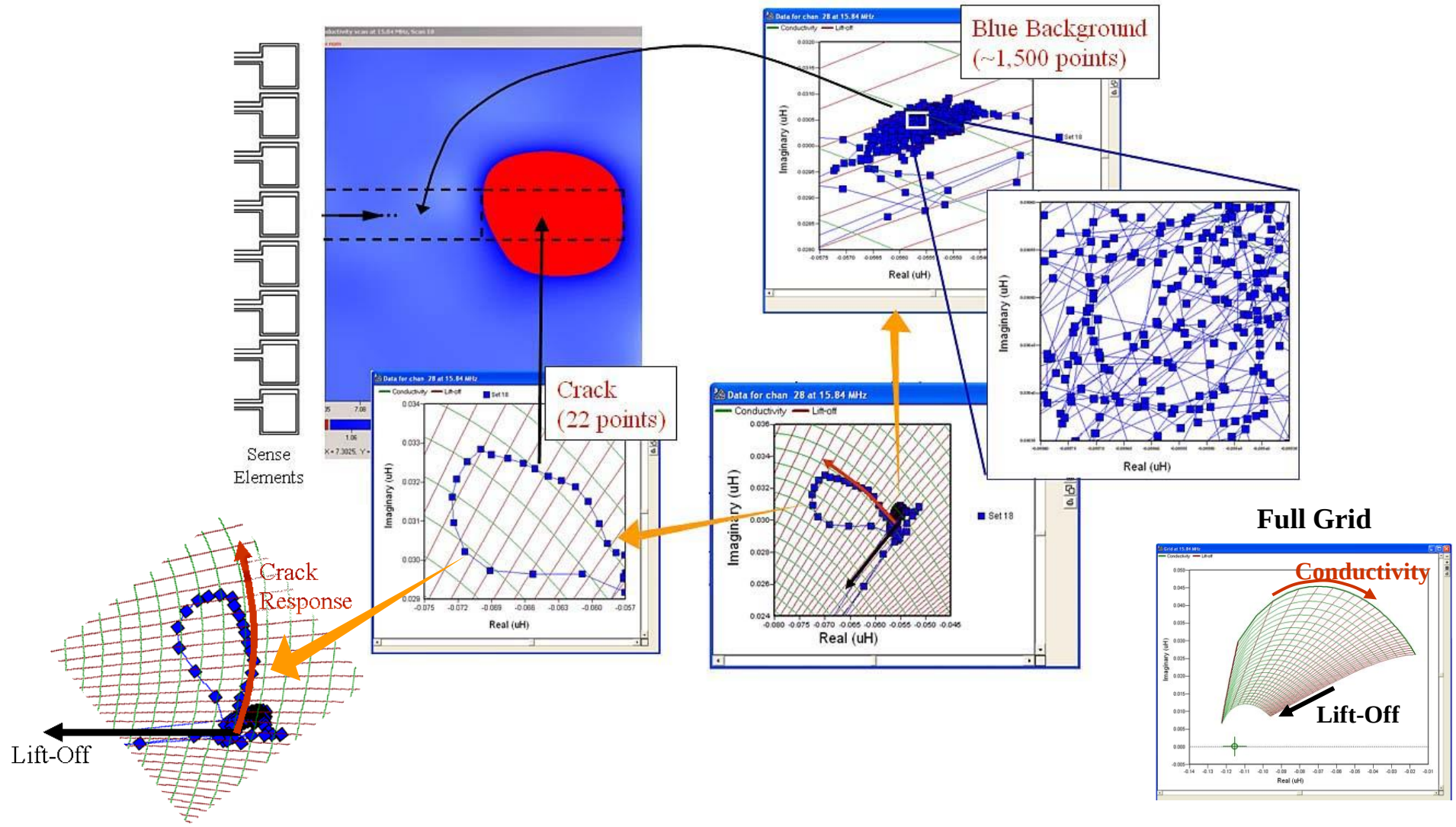

© JENTEK Sensors 2009

Automated Engine Disk Slot Inspection System

- In use at NAVAIR Depot since April 2005
- Disks with verified cracks detected, several of these large and small cracks **not detected by conventional ET and LPT**
- Low False Alarm Rate

Conductivity **Lift-Off**

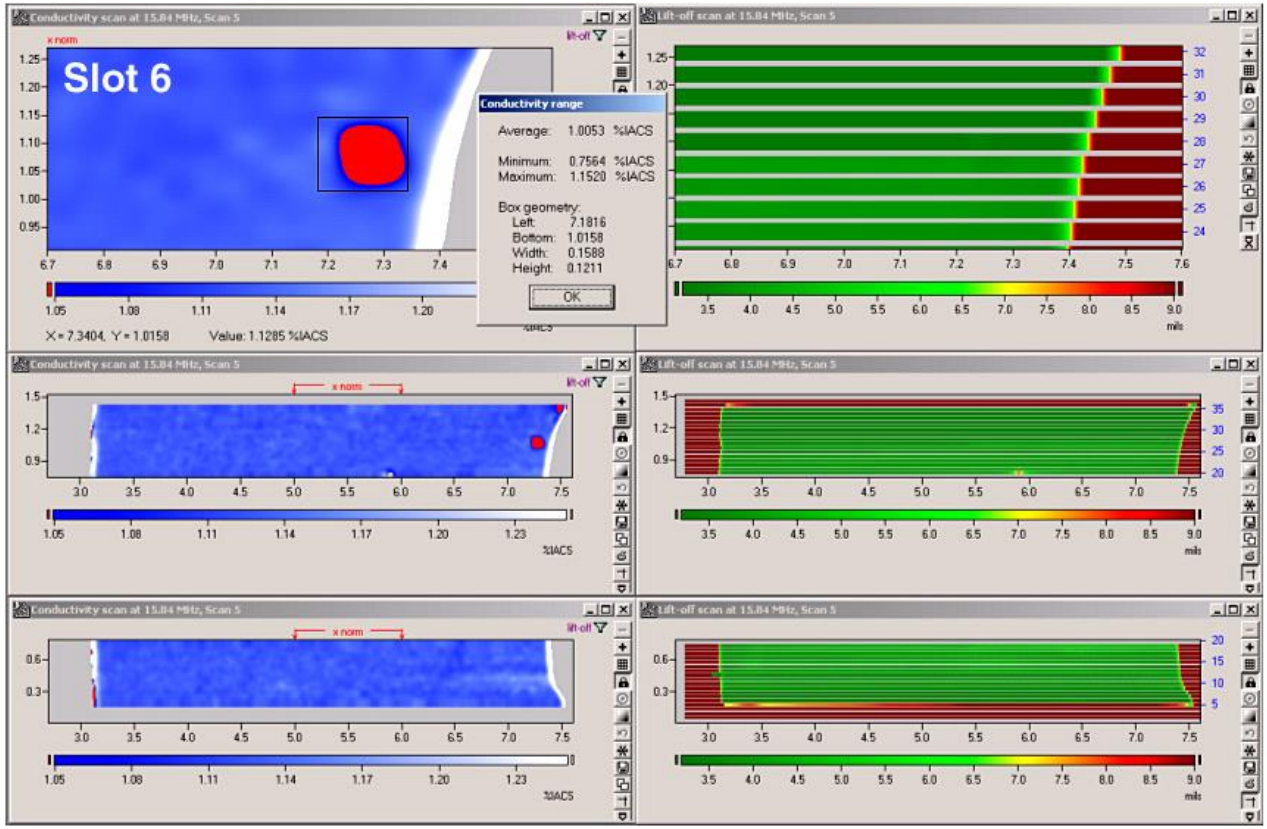

© JENTEK Sensors 2009

â Definitions

$\hat{a}_{\sigma drop}$ *VS* $\hat{a}_{FW@0.95}$

Coupon Fatigue Crack Response (16.9 mils)

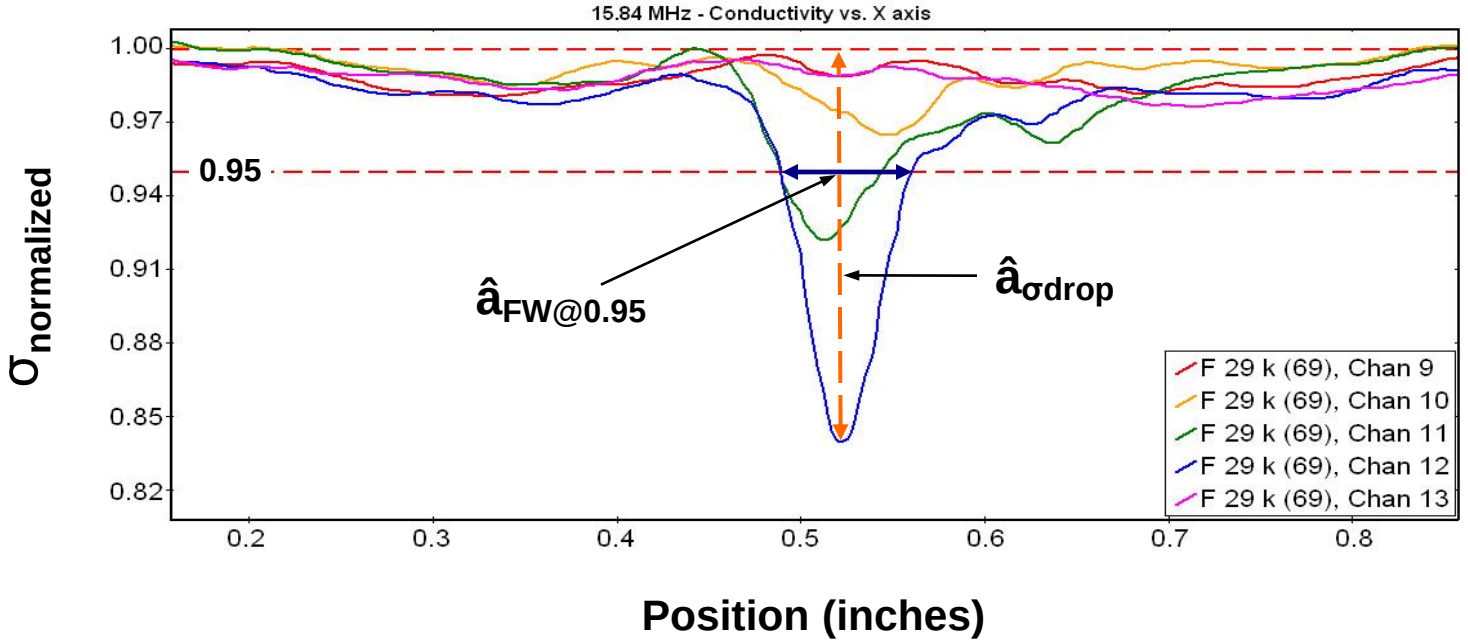

© JENTEK Sensors 2009

â vs a Plots

$\hat{a}_{\sigma drop}$ *vs* $\hat{a}_{FW@0.95}$

Log($\hat{a}_{\sigma drop}$) vs log(a) regression

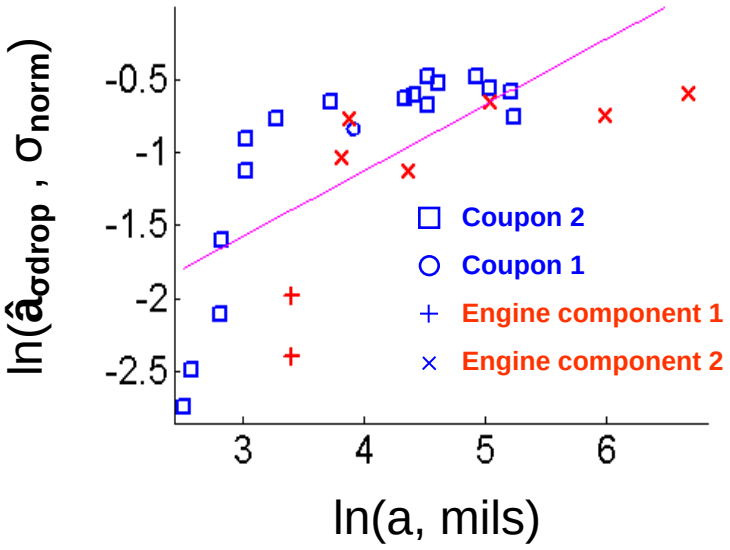

Log($\hat{a}_{FW@0.95}$) vs log(a) regression

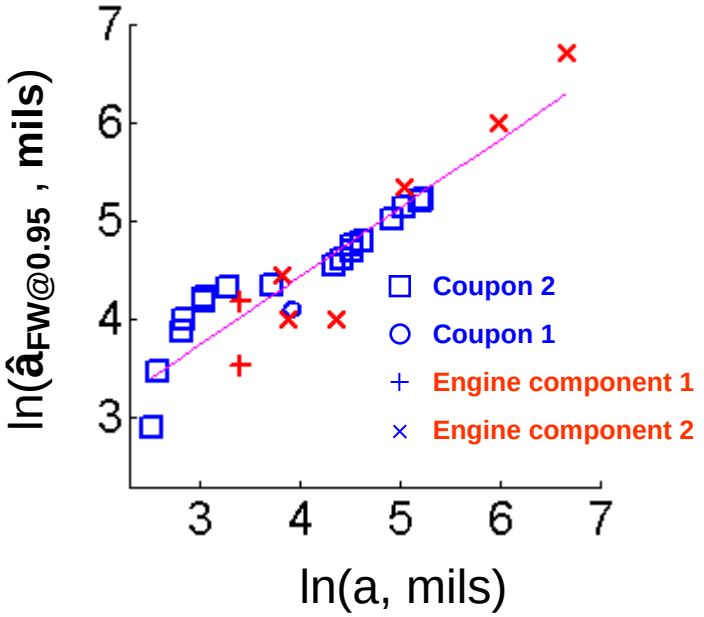

Note: Above a 0.04 in. crack length the $\hat{a}_{FW@0.95}$ definition produces an "unbiased estimator" for crack length. Below 0.02 in. crack lengths multiple small cracks result in a positively biased crack length estimate.

© JENTEK Sensors 2009

Fatigue Specimen and Test Setup (7-Channel FA43)

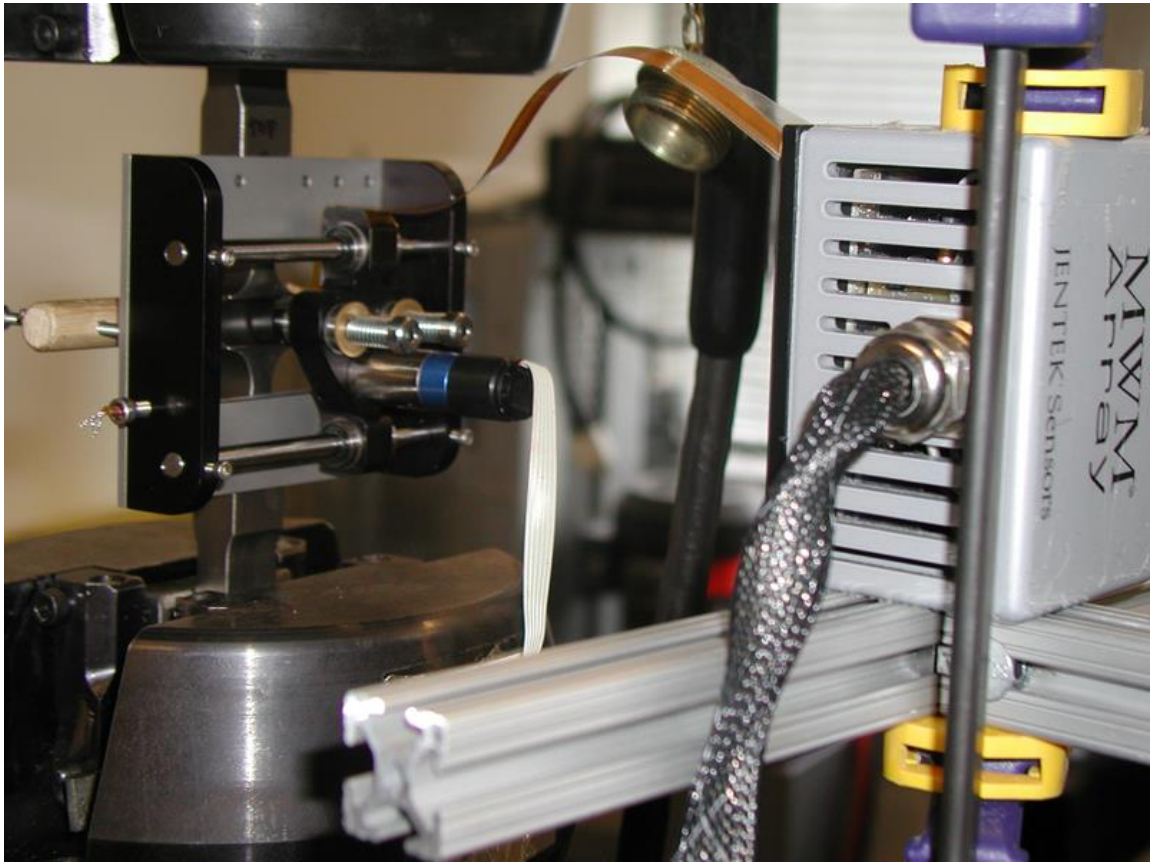

MWM-Array FA43

© JENTEK Sensors 2009

Coupon Example Cracks

Interval	Total Cycles	a, mils
0	0	**0**
2	**6,000**	**3.9**
11	**27,376**	**16.7**
12	**29,041**	**16.9**
25	**41,000**	**186.6**

© JENTEK Sensors 2009

37-Channel MWM-Array FA57

25,376 Cycles

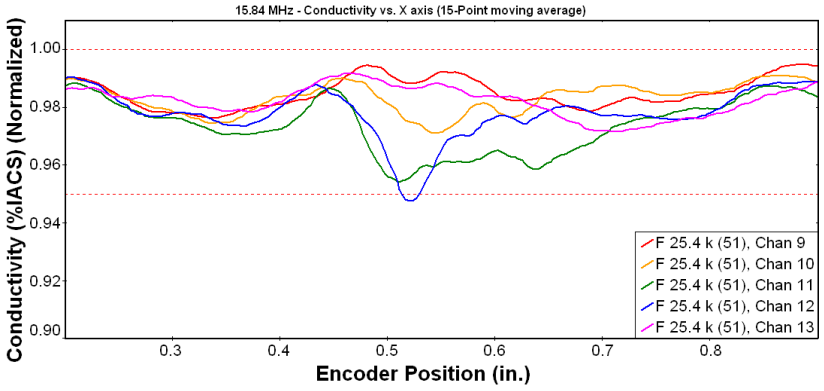

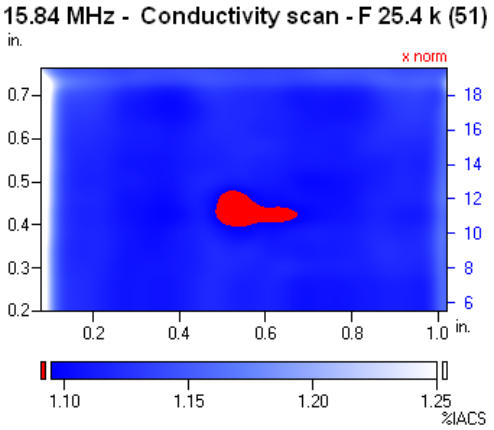

Crack 12.3 mils

26,376 Cycles

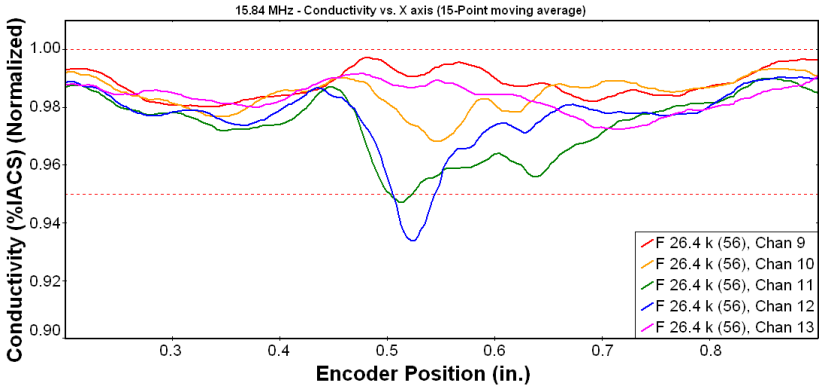

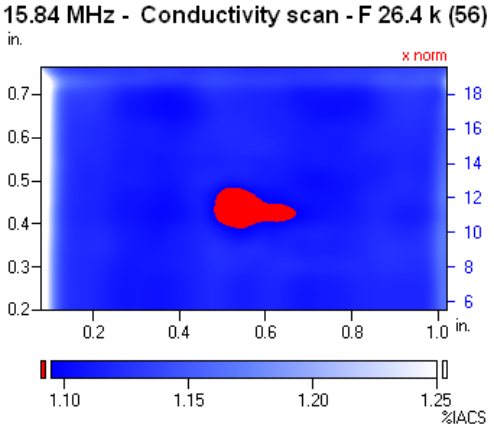

Crack 13.2 mils

27,376 Cycles

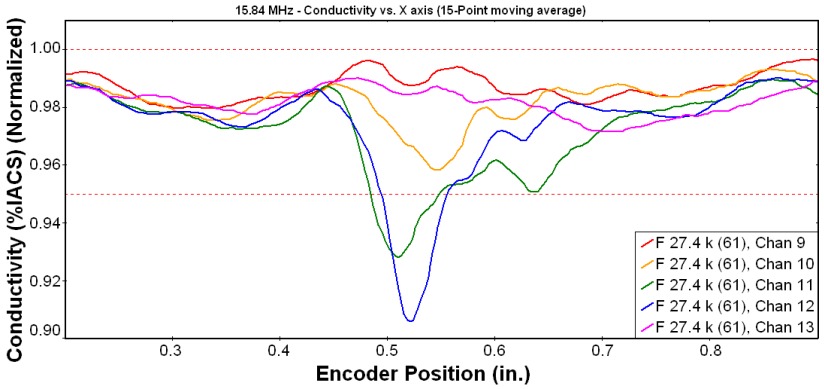

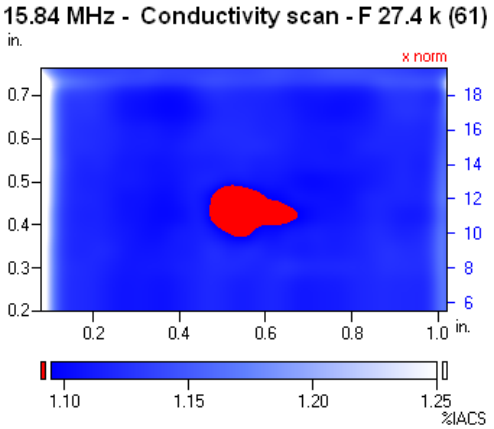

Crack 16.7 mils

© JENTEK Sensors 2009

Difference Imaging Provides Improved Sensitivity, with Averaging of 5 Repeat Scans Reduces Noise

Channel 12

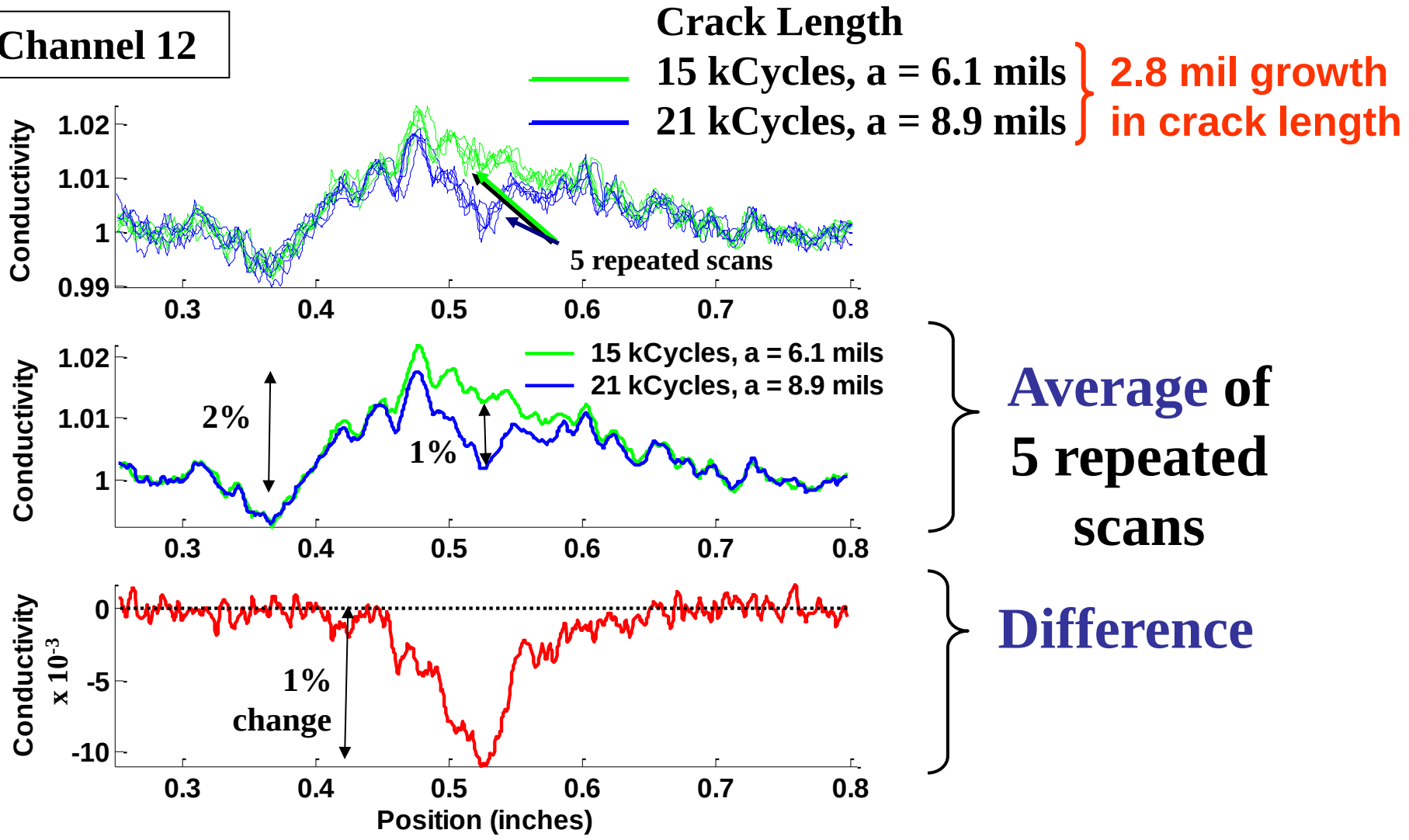

© JENTEK Sensors 2009

15 kCycles, a = 6.1 mils

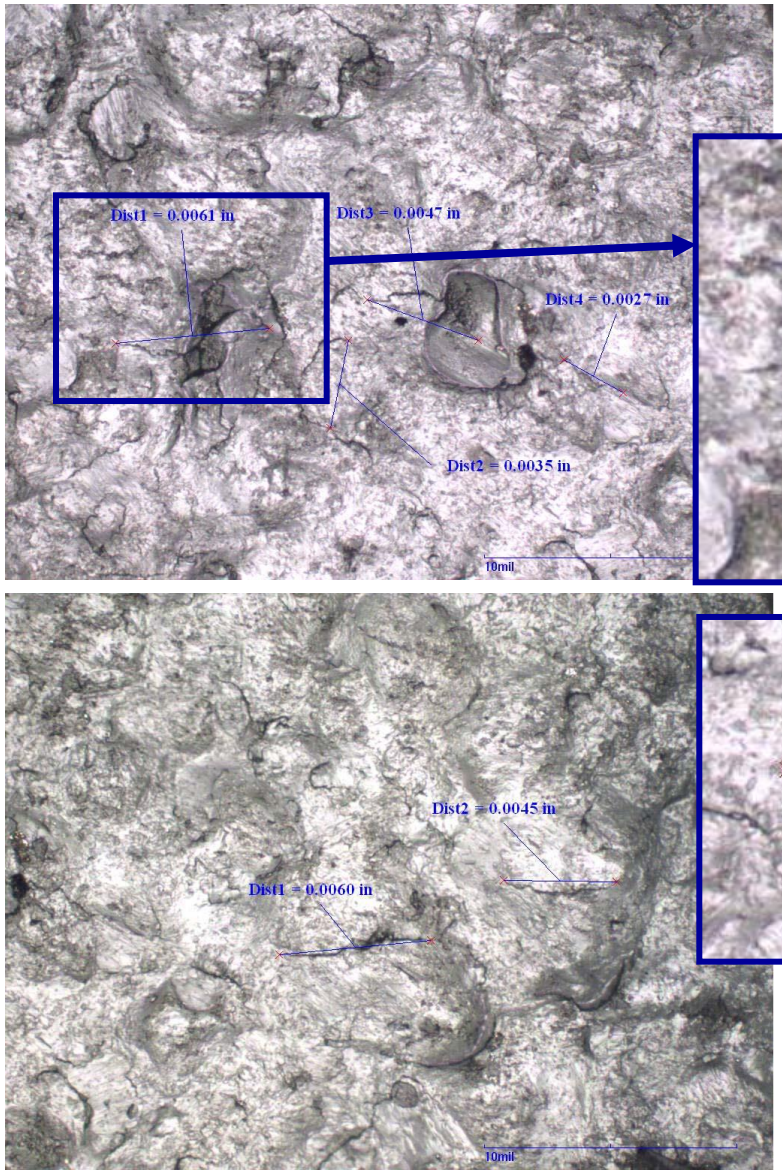

21 kCycles, a = 8.9 mils

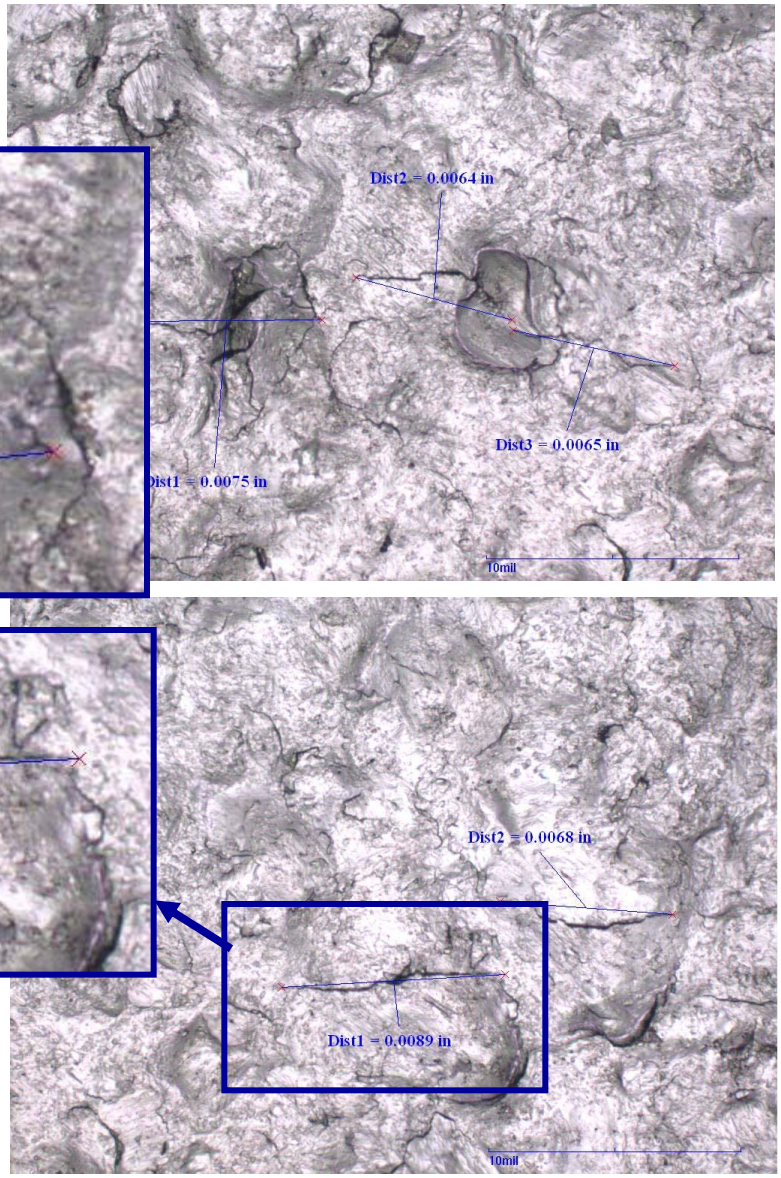

© JENTEK Sensors 2009

Bolt Hole Inspection

- C-Scan Imaging using MWM-Arrays
- Detection of Cracks at Edges with edge location correction
- Spatial Filtering for Cracks at Edges

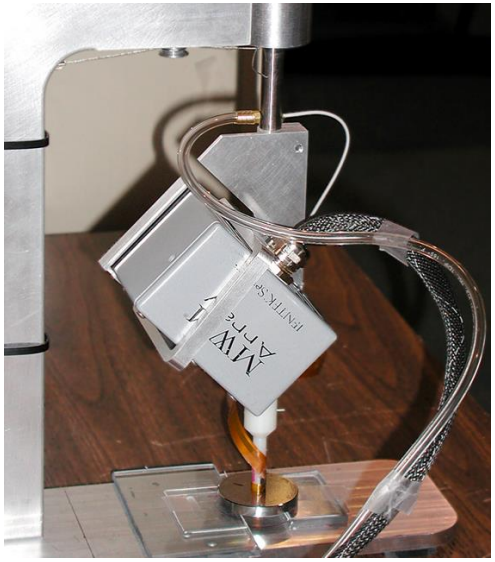

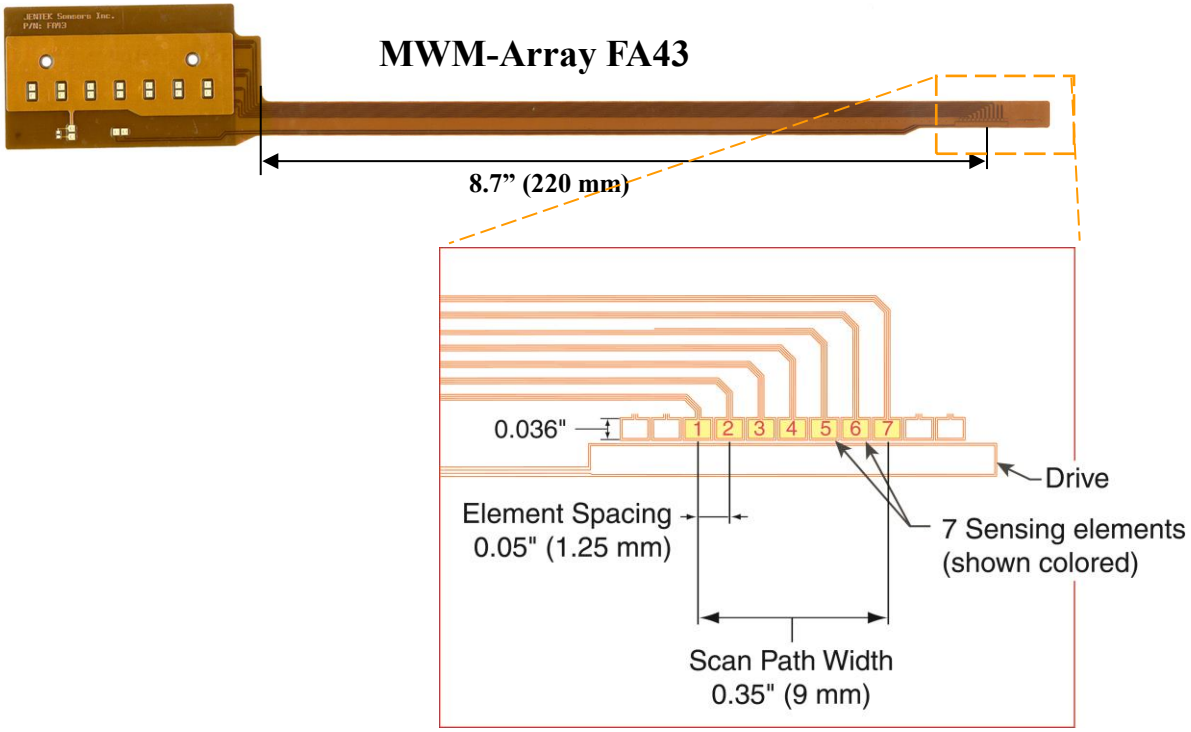

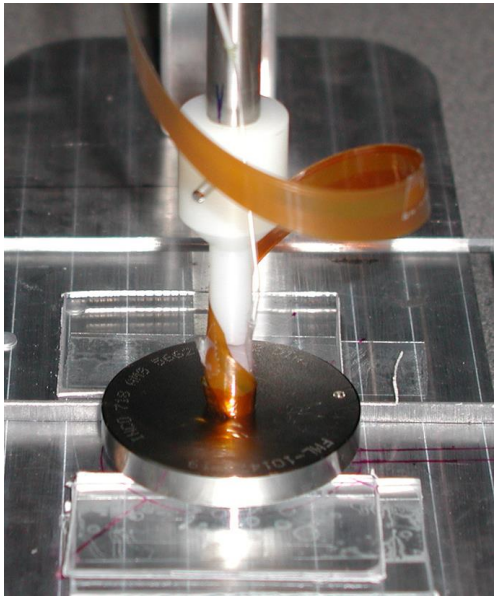

© JENTEK Sensors 2009

Bolt Hole Inspection

Detection of Cracks at Edges with Edge Location Correction

GridStation Conductivity/Lift-Off Images (Unfiltered)

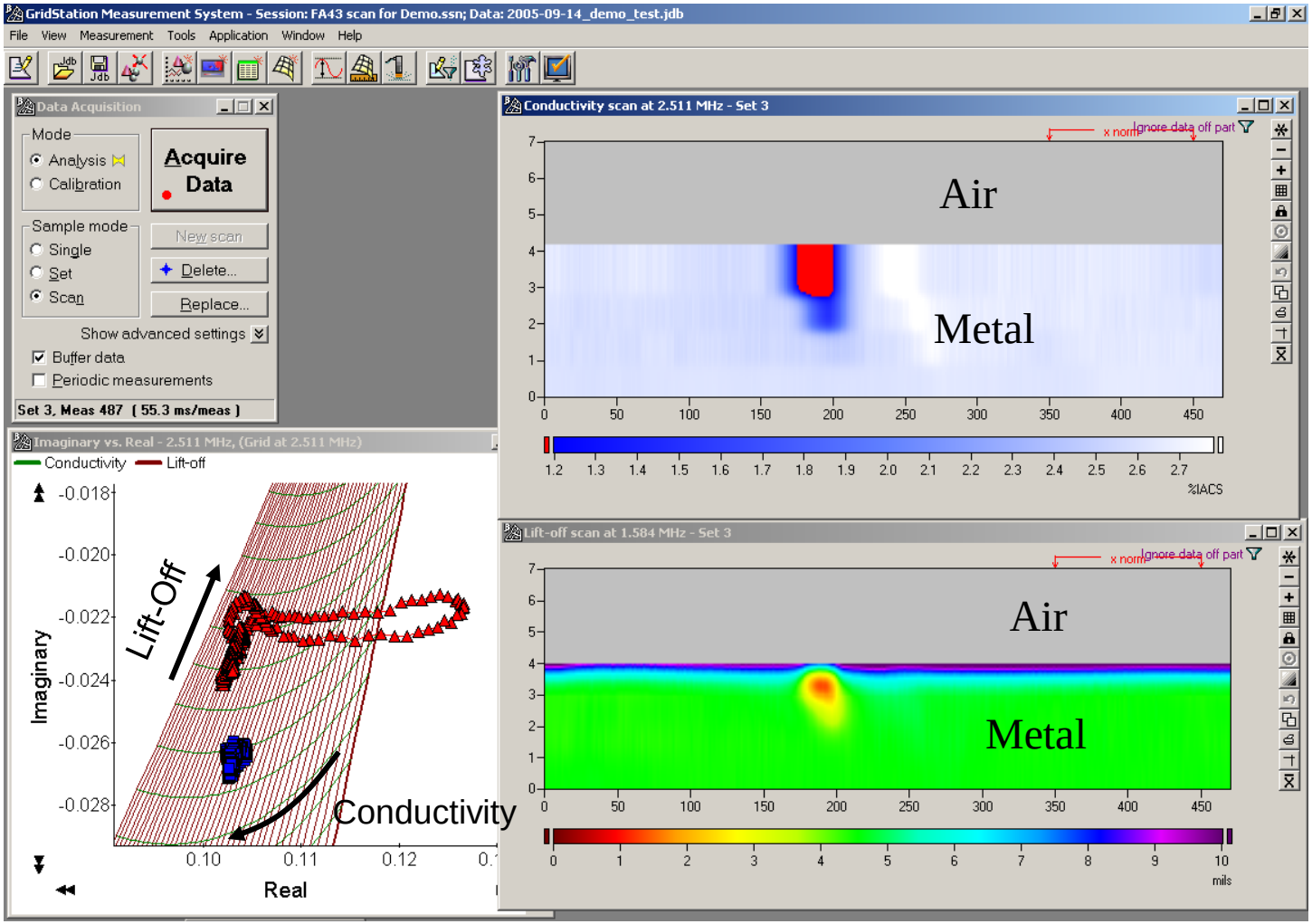

© JENTEK Sensors 2009

Detection of Cracks at Edges with:

- Edge location correction, and
- Spatial Filtering, using Signature Libraries

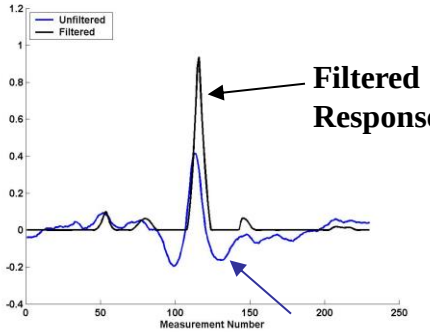

Filtered Response

Conductivity Signature

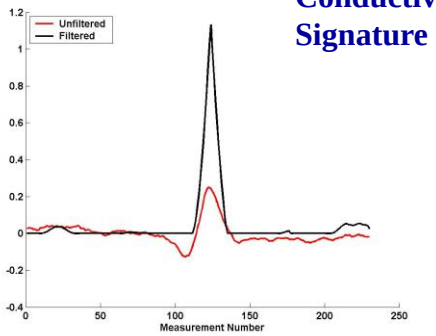

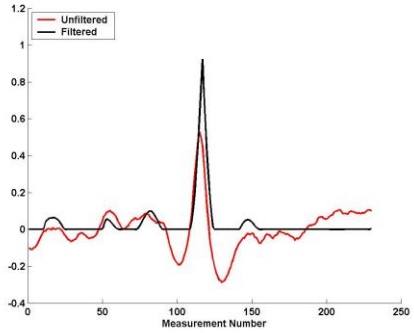

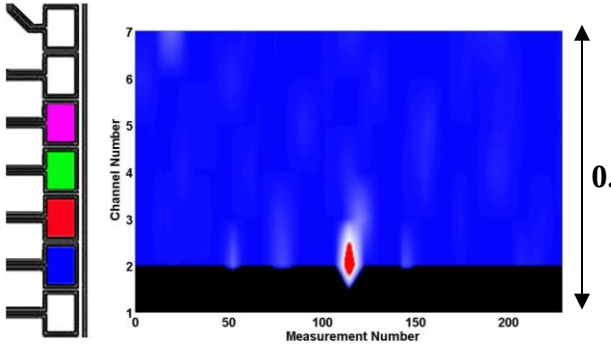

Channel 2, Lift-Off Factor = -0.69

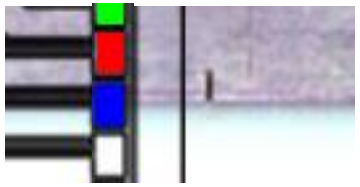

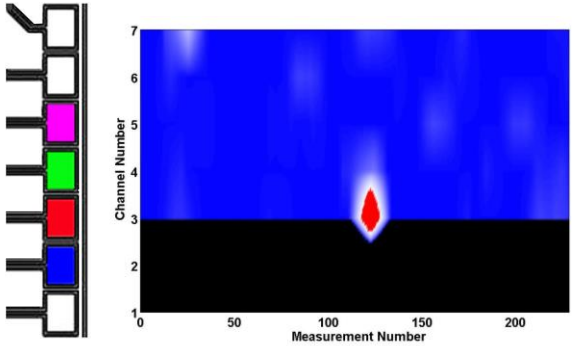

Channel 3, Lift-Off Factor = -0.96

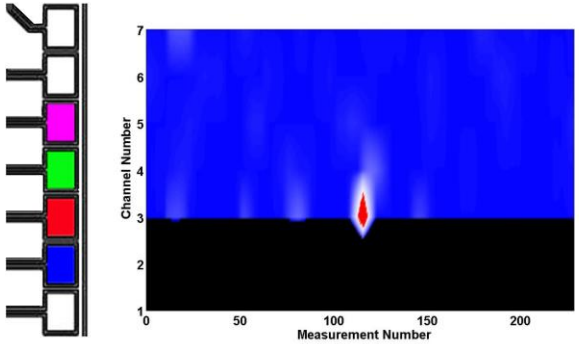

Channel 3, Lift-Off Factor = -0.47

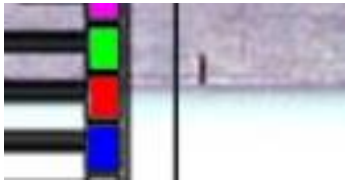

© JENTEK Sensors 2009

Signature Library

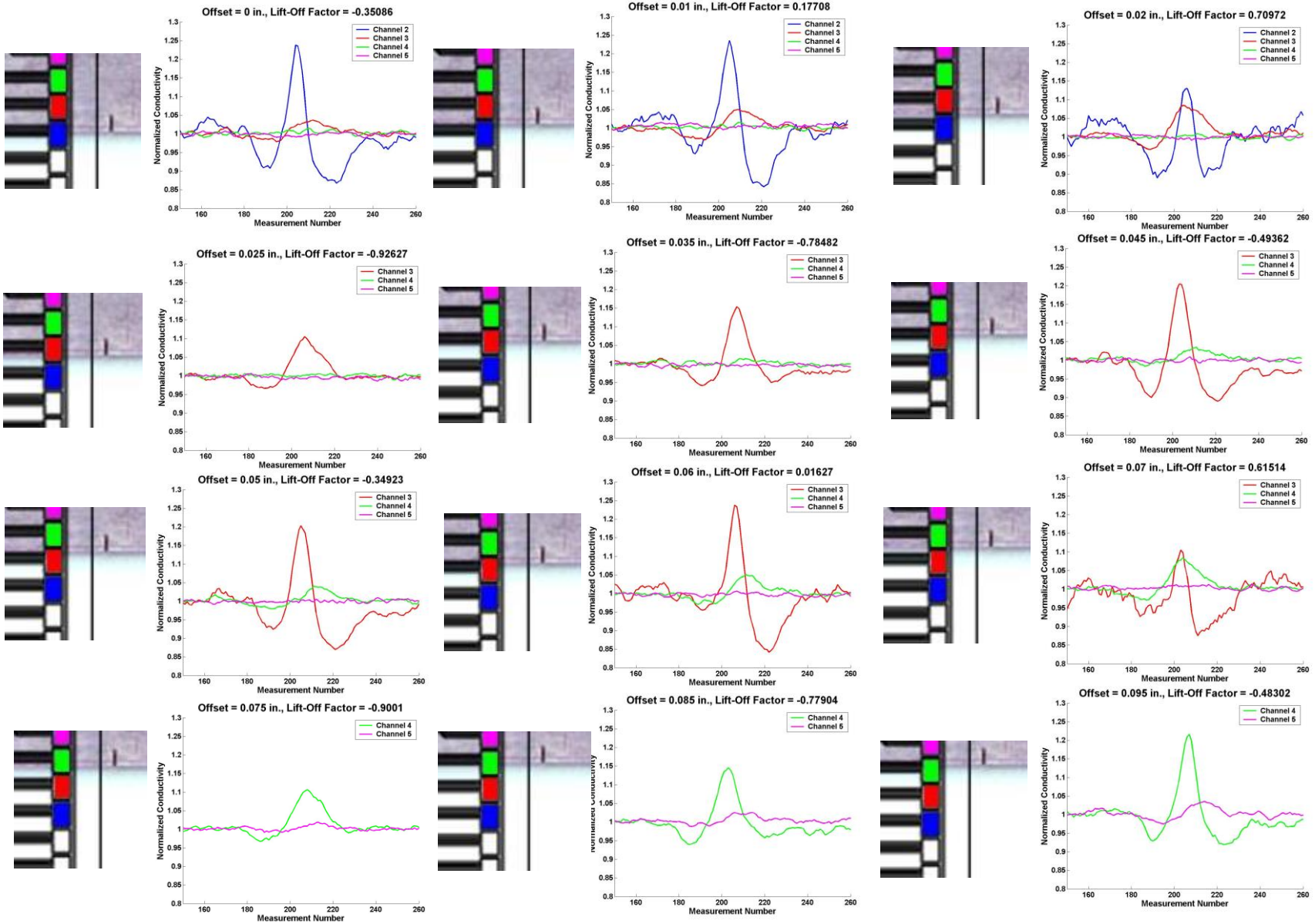

© JENTEK Sensors 2009

ASTM Standard – "Air Calibration"

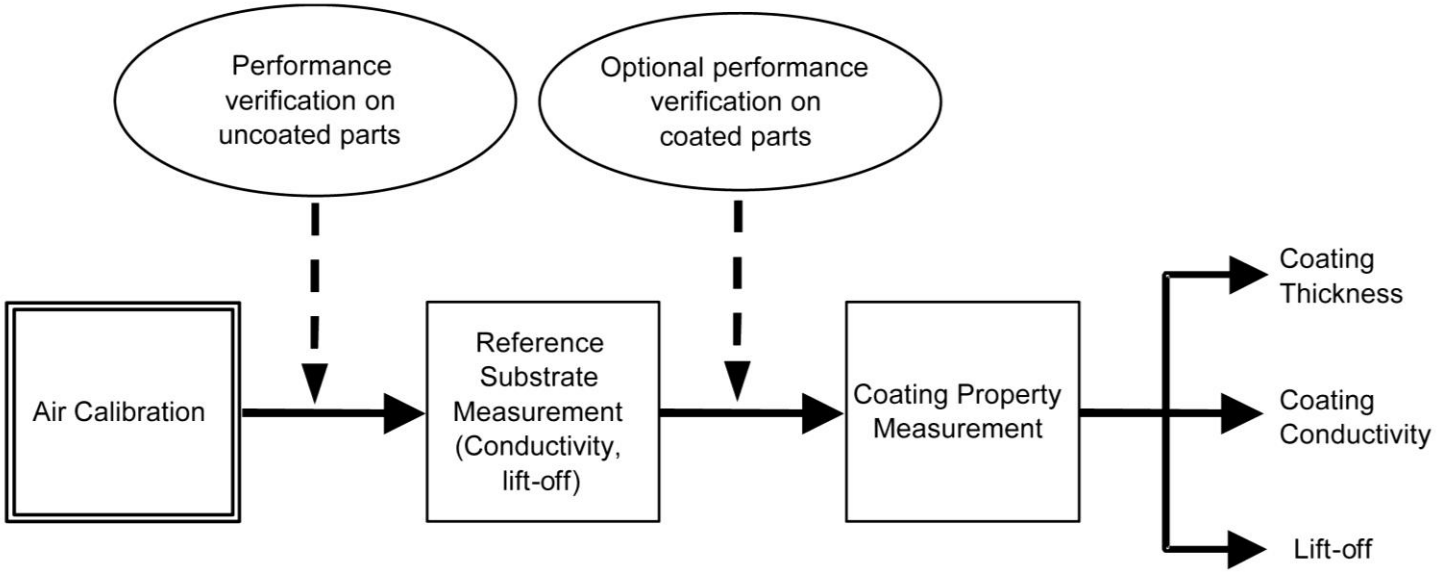

Designation: E 2338 – 04

Standard Practice for Characterization of Coatings Using Conformable Eddy-Current Sensors without Coating Reference Standards[1]

This standard is issued under the fixed designation E 2338; the number immediately following the designation indicates the year of original adoption or, in the case of revision, the year of last revision. A number in parentheses indicates the year of last reapproval. A superscript epsilon (ε) indicates an editorial change since the last revision or reapproval.

© JENTEK Sensors 2009

HyperLattices

(patents issued and pending)

- Measure Four Unknowns
- Provide High Resolution image of each unknown
- Automated & Real-Time

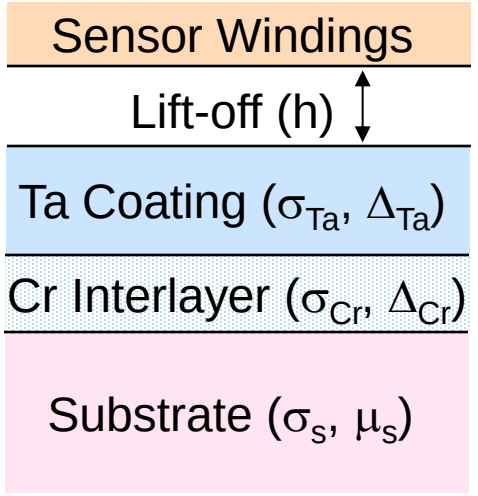

Low *f* σ_{Ta}- Δ_{Ta}- h Lattice

μ_s, σ_s, σ_{Cr}, δ_{Cr} constant

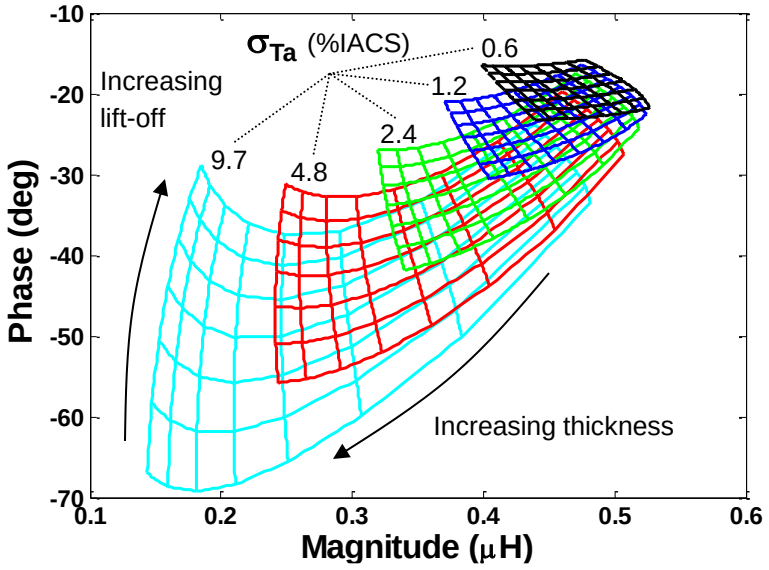

High *f* σ_{Ta}- Δ_{Ta}- h Lattice

μ_s, σ_s, σ_{Cr}, δ_{Cr} constant

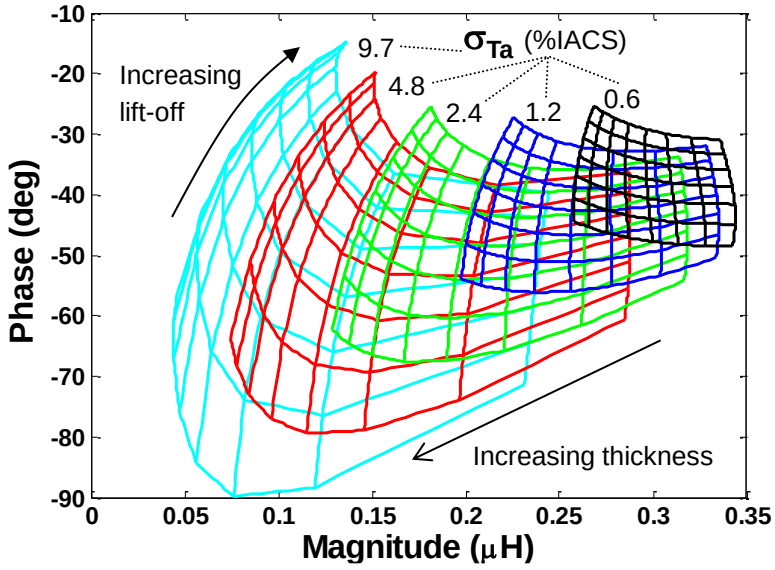

© JENTEK Sensors 2009

Schematics of 4-Unknown Constructs

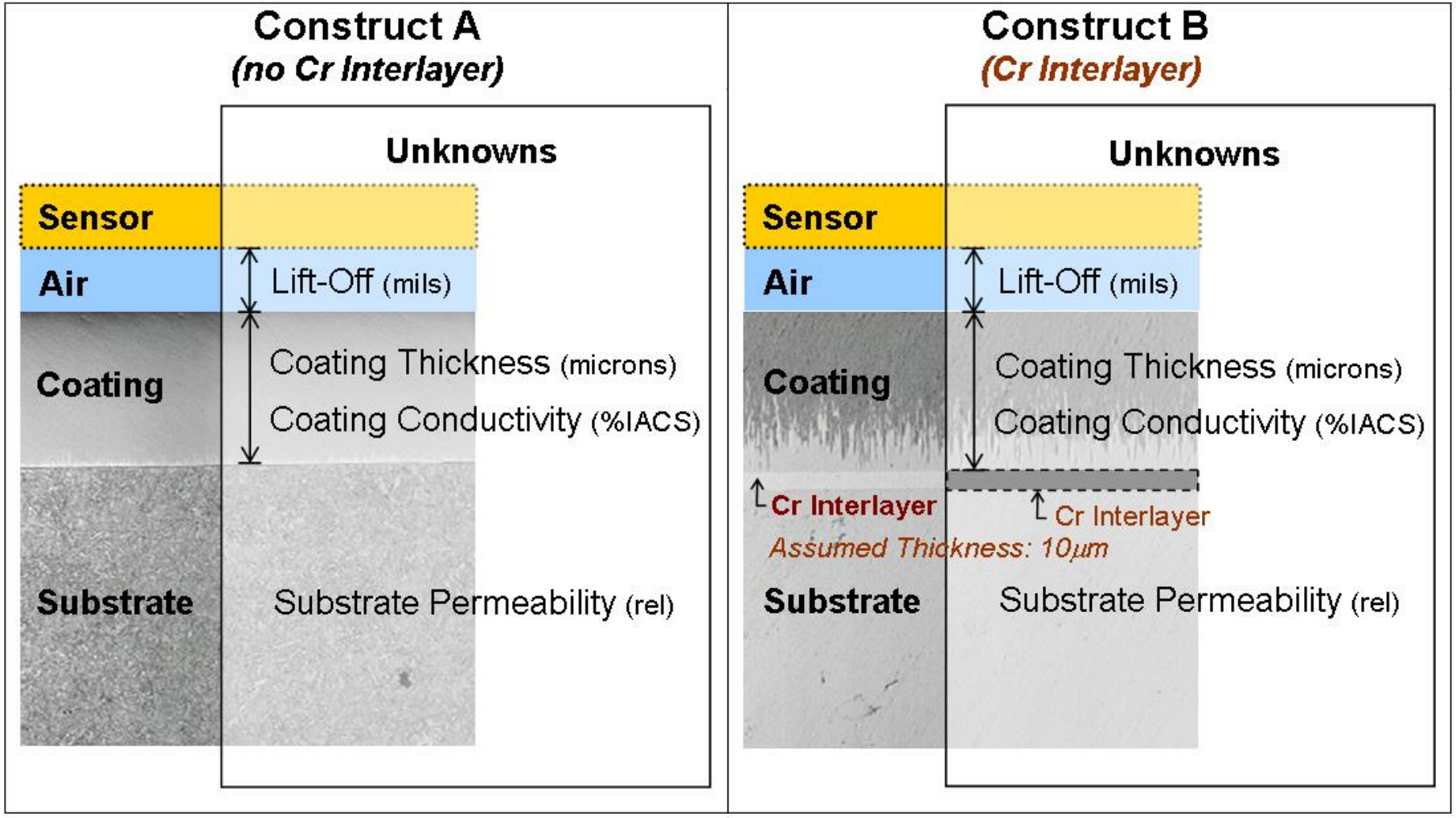

© JENTEK Sensors 2009

Example of MWM-Array Conductivity Image and Corresponding Sample

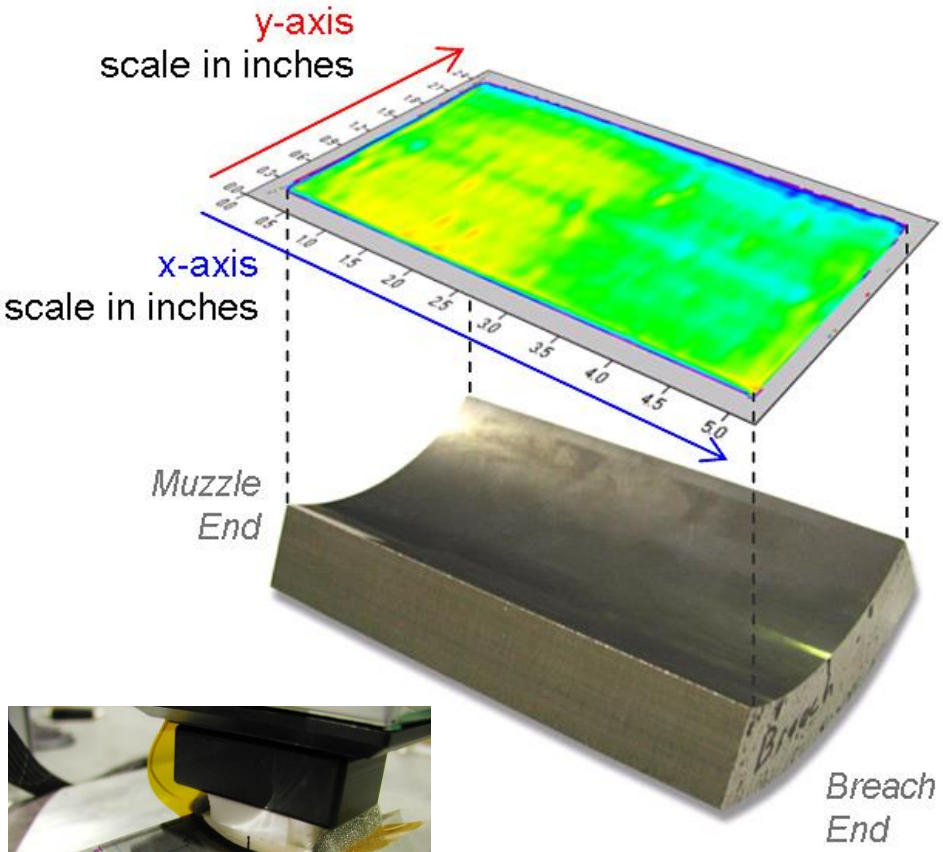

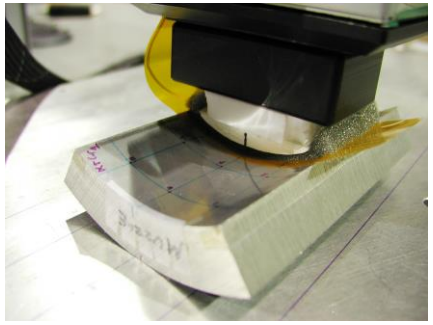

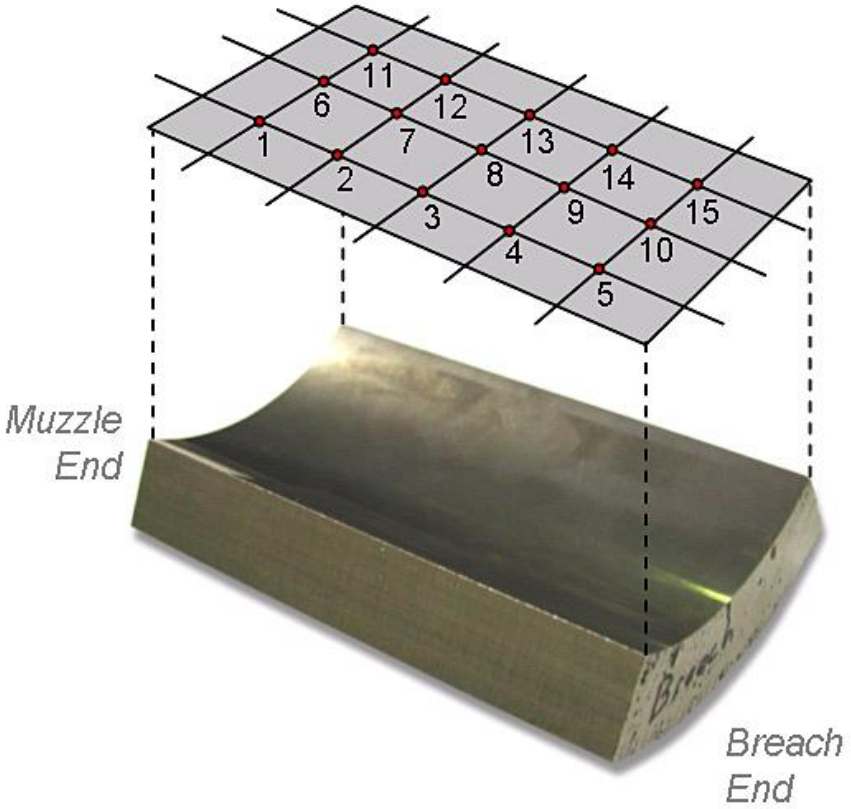

© JENTEK Sensors 2009

Matrix of the Samples Analyzed by JENTEK

			Sputtering Gas	
			Ar	Kr
Coating Composition	Majority α-Tantalum	100% Alpha	X	
		100% Alpha *with Cr*		X
		Mixed Phase (majority alpha)	X	
		Mixed Phase (majority alpha) *with Cr*		X
	Majority β-Tantalum	Mixed Phase (majority beta)		
		Mixed Phase (majority beta) *with Cr*		
		100% Beta	X	
		100% Beta *with Cr*		

Samples

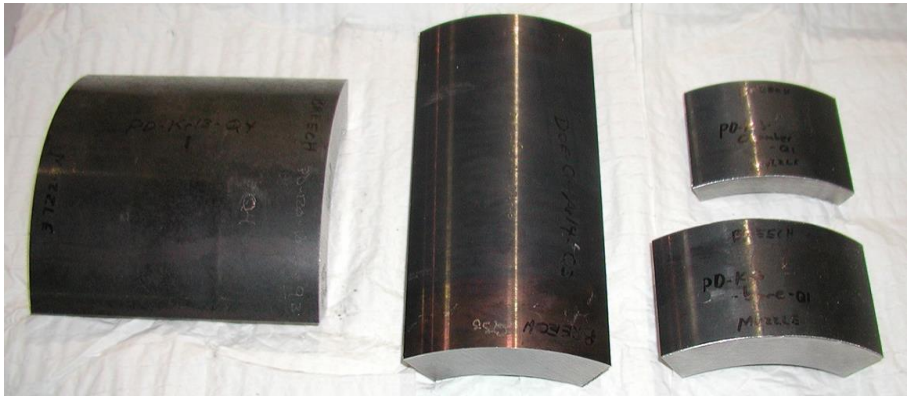

© JENTEK Sensors 2009

Examples of MWM-Array Coating Conductivity Images

Samples Sputtered in Krypton

Sample 4: α-Phase Tantalum with Cr Interlayer

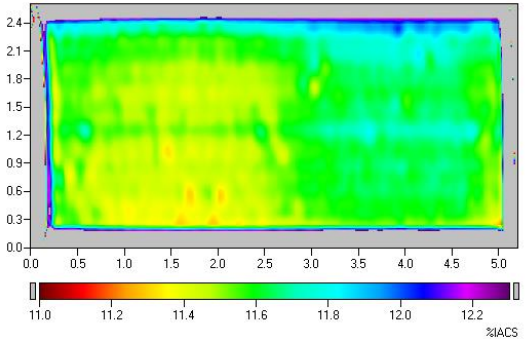

Sample 6: (α + β) Tantalum with Cr Interlayer

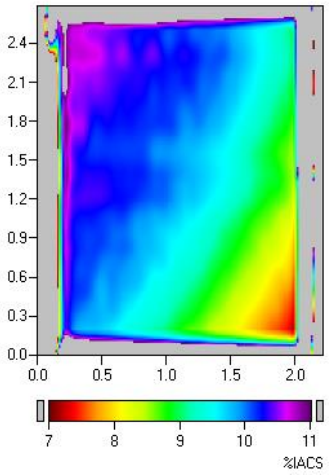

Sample 7: (α + β) Tantalum with Cr Interlayer

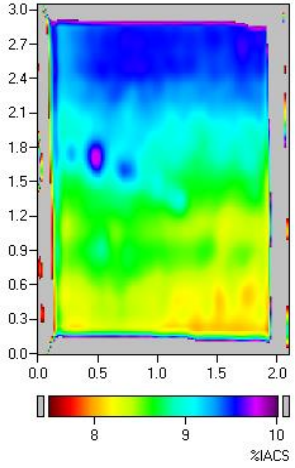

FA28 Scans - Tantalum Coated Gun Barrel Steel

Sample PD-120-Kr10-Q1, 9% Alpha-Ta with Sputtered Cr Interlayer

Tantalum Coating Conductivity *(%IACS)*

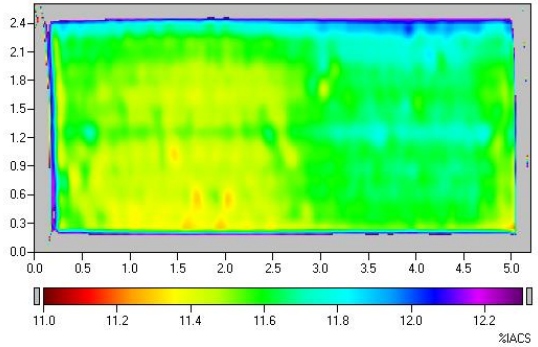

Tantalum Coating Thickness *(microns)*

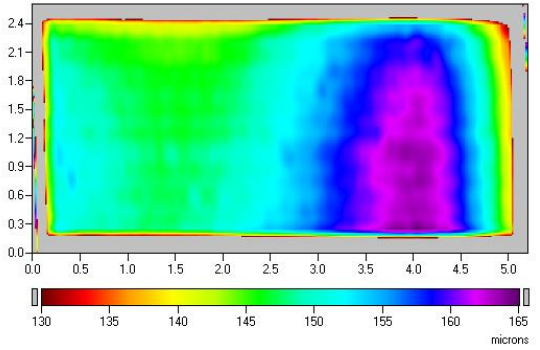

Steel Substrate Permeability *(rel)*

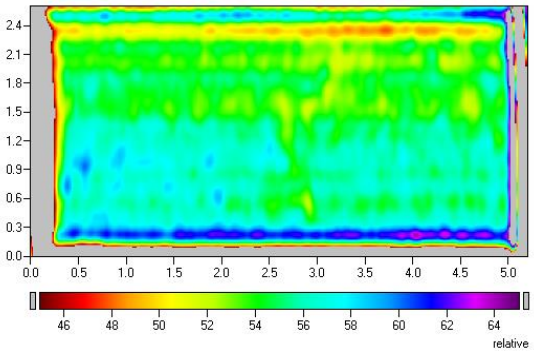

Lift-Off *(mils)*

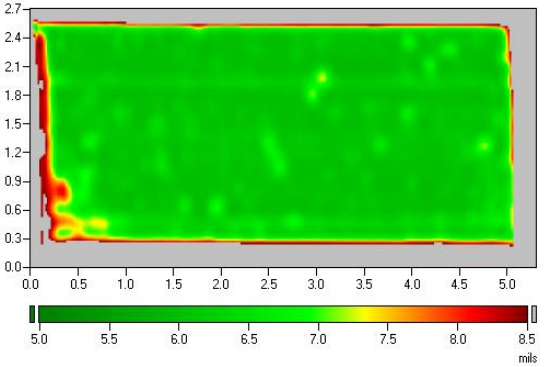

© JENTEK Sensors 2009

MWM-Array Measured Tantalum Coating Thickness Values

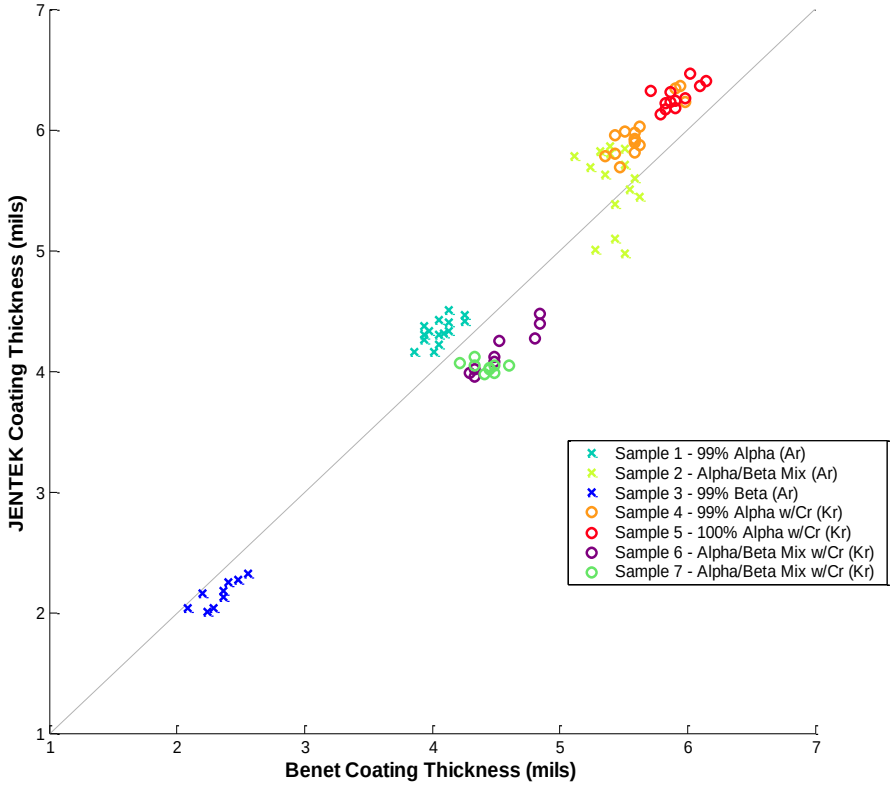

Conductivity vs. Phase Composition for Tantalum Coatings

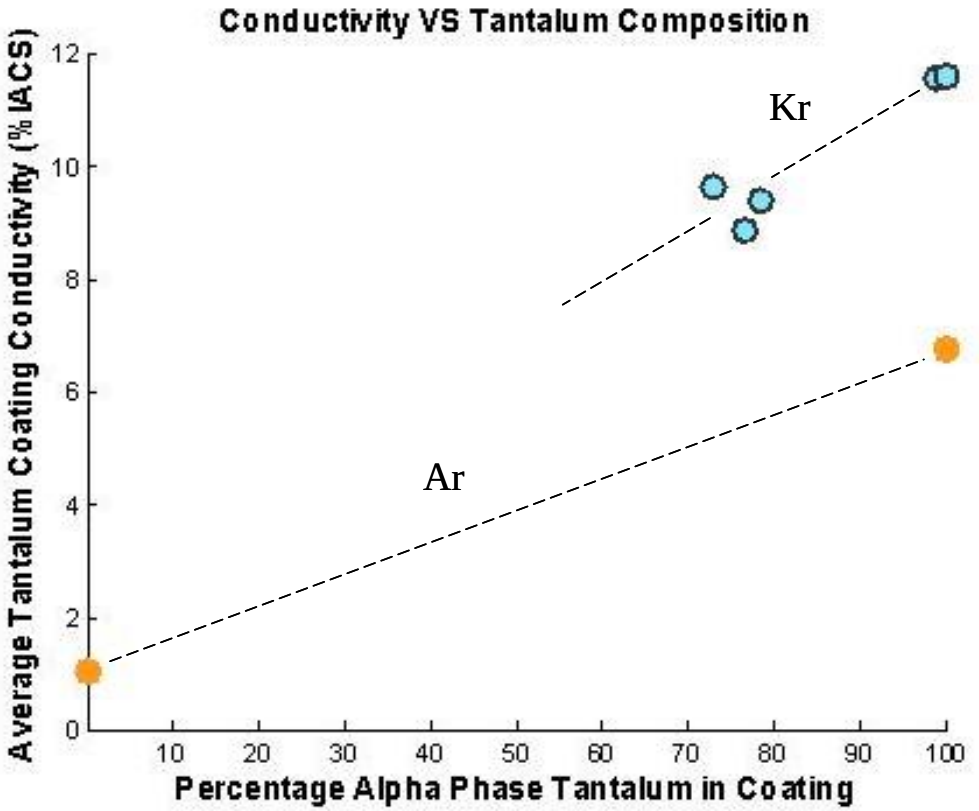

© JENTEK Sensors 2009

Quadri-Directional Magnetic Stress Gage (QD-MSG)

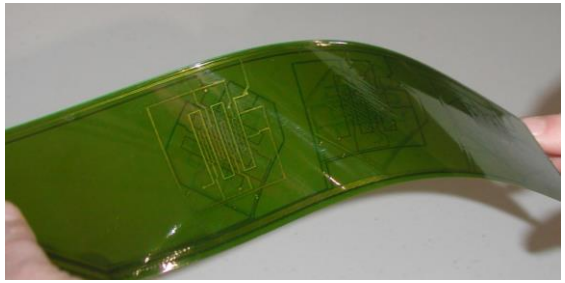

$$\text{Transinductance} = \frac{V_2}{j\omega i_1} = \text{Re}\left(\frac{V_2}{j\omega i_1}\right) + j\ \text{Im}\left(\frac{V_2}{j\omega i_1}\right)$$

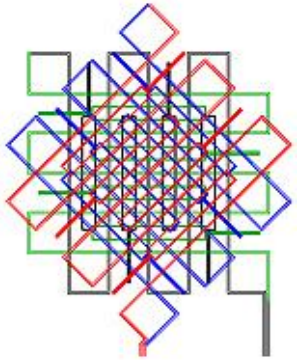

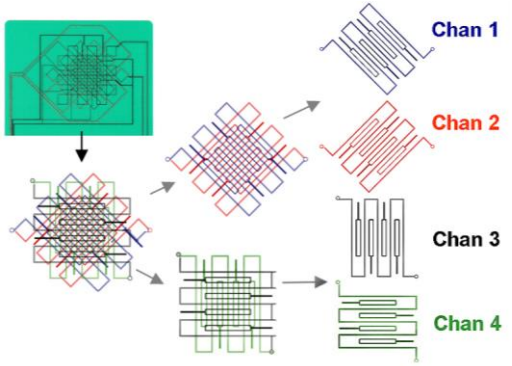

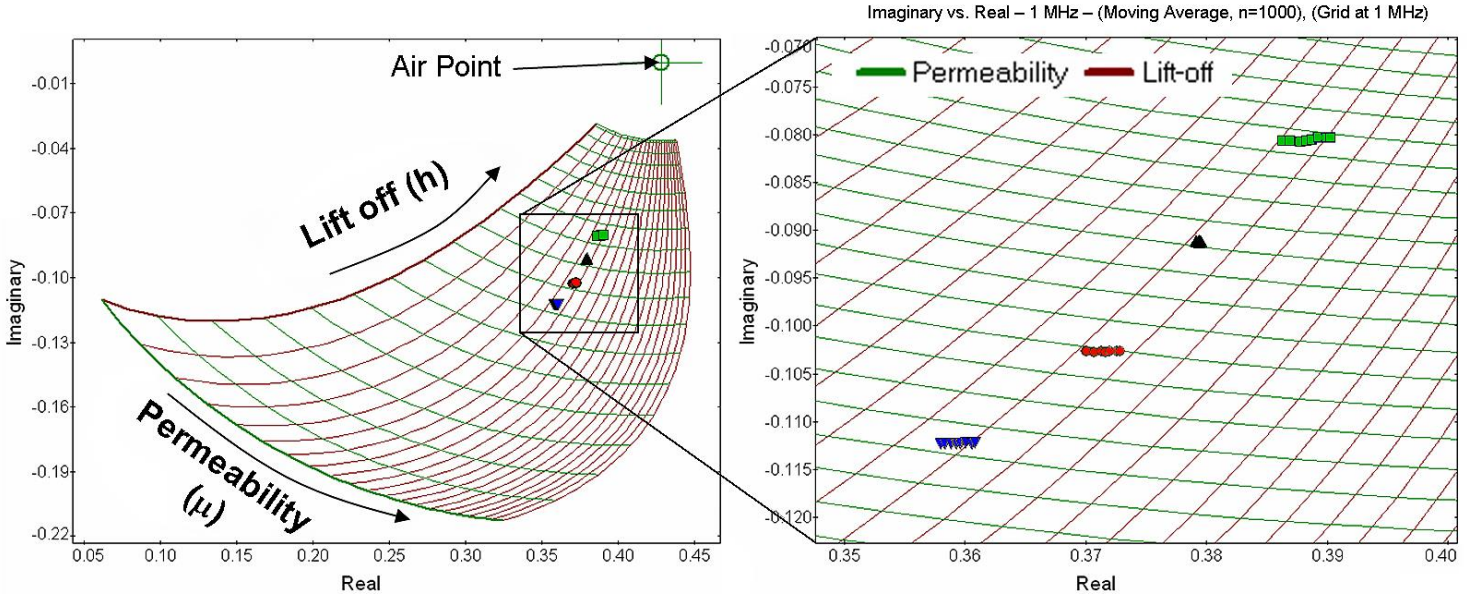

© JENTEK Sensors Inc. All rights Reserved.

QD-MSG Dynamic, Non-Contact Torque Measurement Procedure

Air Calibration

↓

Two-Point (two lift-off) Recalibration

↓

Record Load Ramp Data including Initial No Load Point

↓

Estimate Hysteresis Correction Factors and Permeability-to-Stress Scale Factors

↓

Record No Load Point (or estimate **change** from initial No Load Point)

↓

Estimate Torque, Axial & Bending Loads

Hysteresis Correction
(after temperature correction)

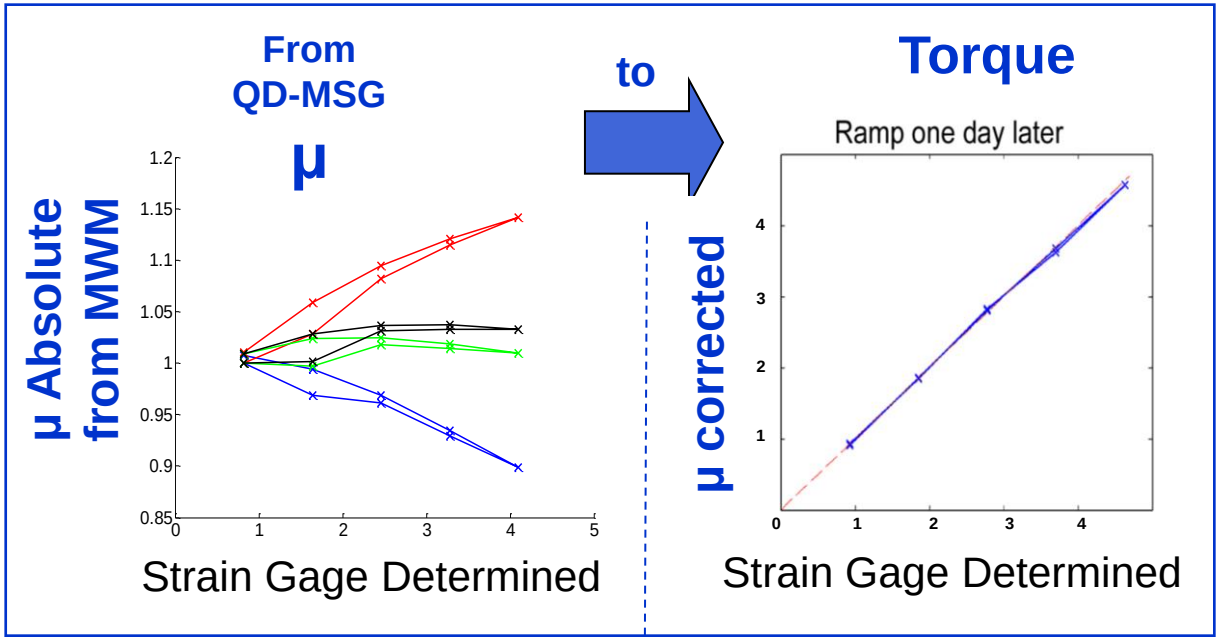

© JENTEK Sensors 2009

Sensor Installation for Full Scale Testing at Boeing, Philadelphia

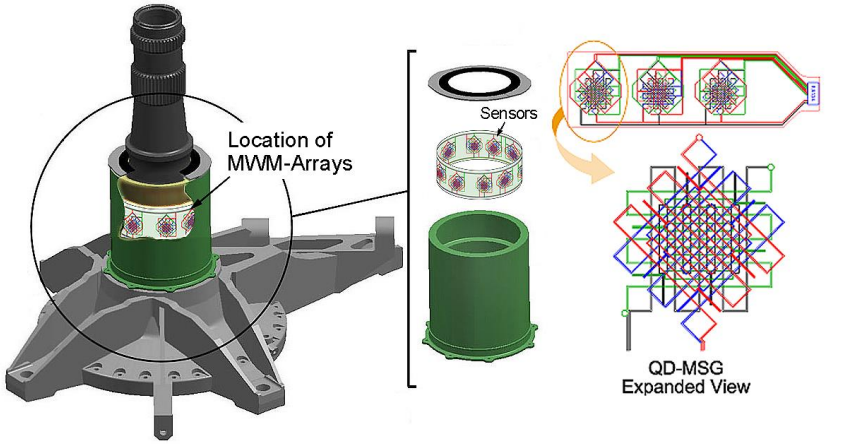

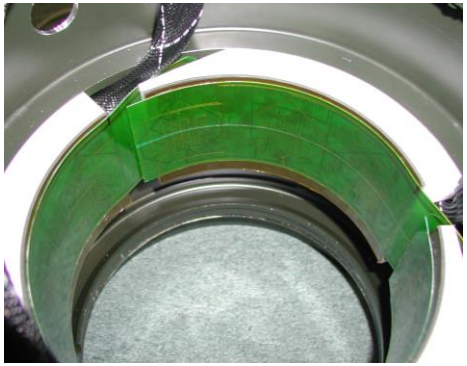

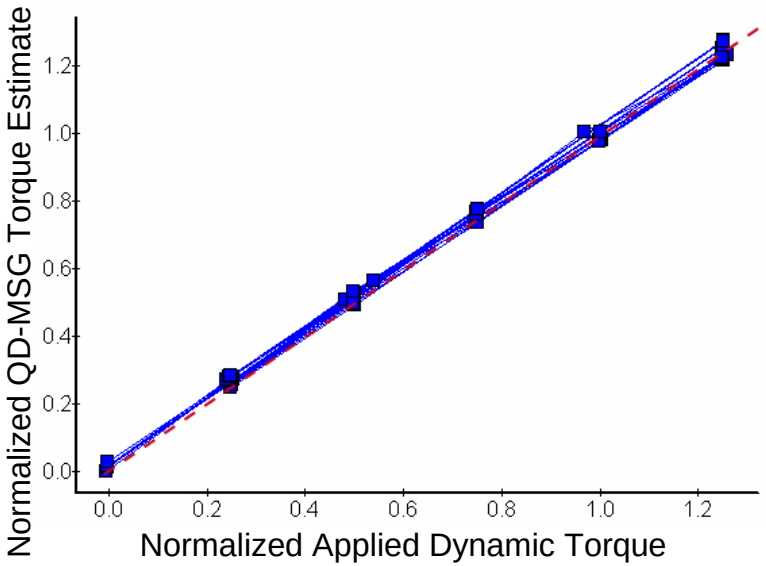

Two Successful Full Scale Tests Completed

© JENTEK Sensors 2009

Eddy Current Micromechanical Model (for Composites)

- **Eddy current extension of micromechanical models**
  - Uniaxial fiber bundle model that accounts for magnetic field interactions with the fibers in each orientation.
  - Effective complex permeability accounts for frequency dependence and anisotropic material properties
- **In the process of incorporating the composite model into rapid layered media models.**

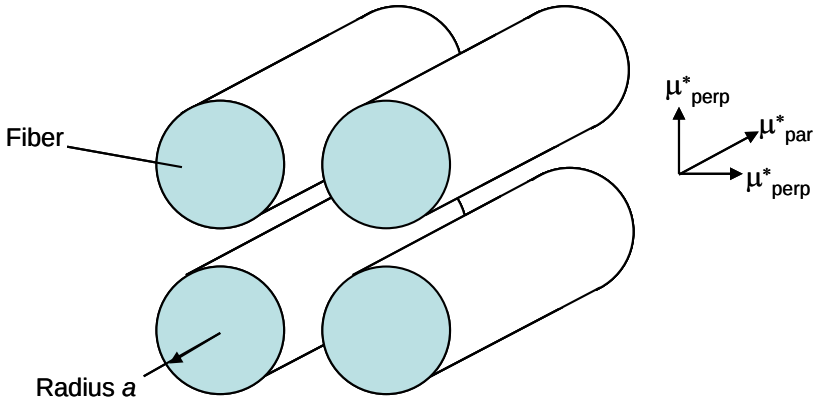

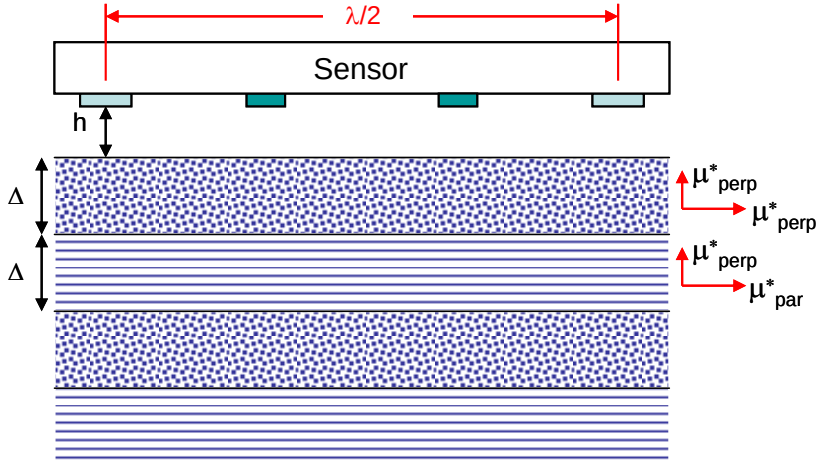

© JENTEK Sensors 2009

A Two Part Presentation

Dr. Neil Goldfine

Introduction to:

- Design, Calibration, Measurement, Inverse Methods, Filters, Decisions
- MWM and MWM-Array Sensors & IDED and IDED-Array Sensors
- Applications (cracks, coatings, corrosion, stress, temperature)
  - Grids and Lattices for Multivariate Inverse Methods
  - Air and Reference Calibration
  - Signature Libraries & Time-Sequenced Imaging for Enhanced Detection

Motivation & Applications

Dr. Yanko Sheiretov

Background on:

- Sensor Model
  - Two-port Impedance Matrices, Transimpedance, Maxwell's Equations, Quasistatic Regimes, EM-field Partial Differential Equations and Solutions
- Multivariate Inverse Methods
  - Searching in multi-dimensional nonlinear spaces
  - Multi-dimensional nonlinear interpolation

Physics & Details

© JENTEK Sensors 2009

Basic Circuit Elements

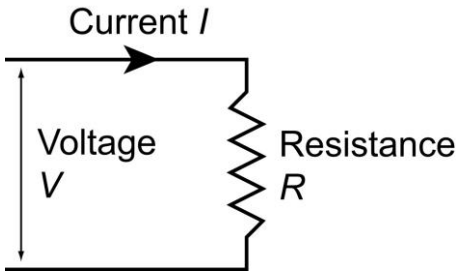

$$V = RI$$ (Ohm's Law)

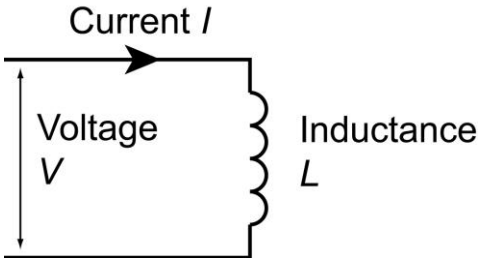

$$V = L\frac{dI}{dt}$$

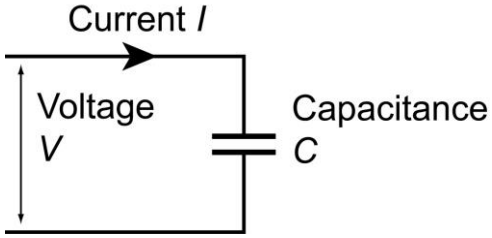

$$I = C\frac{dV}{dt}$$

© JENTEK Sensors 2009

Complex Impedance

Sinusoidal Steady State

$$f(t) = F\cos(2\pi ft + \phi) \Rightarrow f(t) = \Re\left\{\hat{F}e^{j2\pi ft}\right\} = \Re\left\{Fe^{j(2\pi ft+\phi)}\right\}$$

$$\hat{F} = Fe^{j\phi}$$

F = magnitude, ϕ = phase, f = frequency

$$V = RI \Rightarrow \hat{V} = R\hat{I}$$

$$V = L\frac{dI}{dt} \Rightarrow \hat{V} = j2\pi fL\hat{I}$$

$$I = C\frac{dV}{dt} \Rightarrow \hat{V} = \frac{1}{j2\pi fC}\hat{I}$$

Everything can be treated as a simple resistor, using complex numbers

$$\hat{V} = \hat{Z}\hat{I}$$

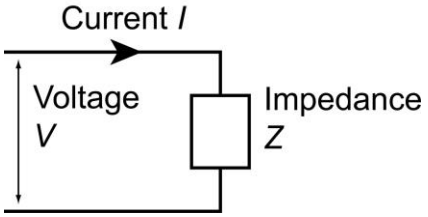

$$\frac{d}{dt} \Rightarrow j2\pi f$$

Drop the hats (^) from now on

© JENTEK Sensors 2009

Two-port Impedance Matrices, Transimpedance

It is difficult to measure the voltage and current at the same set of terminals;
…this is why the MWM and IDED use secondary windings/electrodes.

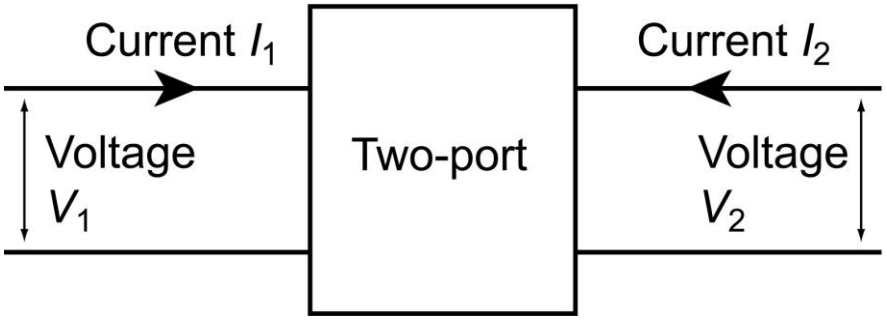

Impedance matrix:

$$\begin{pmatrix} V_1 \\ V_2 \end{pmatrix} = \begin{pmatrix} Z_{11} & Z_{12} \\ Z_{21} & Z_{22} \end{pmatrix} \begin{pmatrix} I_1 \\ I_2 \end{pmatrix}$$

transimpedance

$$\begin{pmatrix} Y_{11} & Y_{12} \\ Y_{21} & Y_{22} \end{pmatrix} = \begin{pmatrix} Z_{11} & Z_{12} \\ Z_{21} & Z_{22} \end{pmatrix}^{-1} \qquad Y_{21} \neq Z_{21}^{-1}$$

$$\begin{pmatrix} I_1 \\ I_2 \end{pmatrix} = \begin{pmatrix} Y_{11} & Y_{12} \\ Y_{21} & Y_{22} \end{pmatrix} \begin{pmatrix} V_1 \\ V_2 \end{pmatrix}$$

transadmittance

MWM: $I_2 = 0 \quad \Rightarrow \quad V_2 = Z_{21} I_1$

IDED: $V_2 = 0 \quad \Rightarrow \quad I_2 = Y_{21} V_1$

The sensors and instrument are designed in a way that requires only one matrix element to be computed.

© JENTEK Sensors 2009

Maxwell's Equations, Quasistatic Regimes

$\nabla \cdot \varepsilon \mathbf{E} = \rho$ Gauss' Law

$\nabla \cdot \mu \mathbf{H} = 0$

$\nabla \times \mathbf{E} = -\frac{\partial \mu \mathbf{H}}{\partial t}$ Faraday's Law

$\nabla \times \mathbf{H} = \mathbf{J} + \frac{\partial \varepsilon \mathbf{E}}{\partial t}$ Ampère's Law

$\nabla \cdot \mathbf{J} + \frac{\partial \rho}{\partial t} = 0$ Charge conservation

Magnetoquasistatic (MWM)

Ignore changing electric fields

$\nabla \cdot \mu \mathbf{H} = 0 \quad \nabla \times \mathbf{H} = \mathbf{J}$

Eddy Currents!

$\nabla \times \mathbf{E} = -\frac{\partial \mu \mathbf{H}}{\partial t}$

If we let $\mu \mathbf{H} = \nabla \times \mathbf{A}$ and $\mathbf{J} = \sigma \mathbf{E}$ (Ohm's Law)

$$\nabla^2 \mathbf{A} = \mu\sigma \frac{\partial \mathbf{A}}{\partial t}$$

Magnetic Diffusion Equation

Electroquasistatic (IDED)

Ignore changing magnetic fields

$\nabla \cdot \varepsilon \mathbf{E} = \rho \quad \nabla \times \mathbf{E} = 0 \quad \nabla \cdot \mathbf{J} + \frac{\partial \rho}{\partial t} = 0$

If we let $\mathbf{E} = -\nabla \Phi$ then

$$\nabla^2 \Phi = -\frac{\rho}{\varepsilon}$$

Poisson's Equation

© JENTEK Sensors 2009

EM-field Partial Differential Equations and Solutions

Writing the equations with complex number notation:

Magnetoquasistatic (MWM)

$$\nabla^2 \mathbf{A} = j2\pi f \mu\sigma \mathbf{A}$$

Electroquasistatic (IDED)

$$\nabla^2 \Phi = 0$$ (no free charge, $\rho = 0$)

Solving these equations in general is very difficult. However, if we assume that:

- The sensor is periodic in the *x*-direction with period (wavelength) λ
- Nothing changes in the *y*-direction and currents flow in the *y*-direction
- The materials are uniform

then we can find some "simple" solutions (periodic in *x*, exponential in *z*):

$$\mathbf{A} \propto \left\{ \begin{matrix} \cos(2\pi x/\lambda) \\ \sin(2\pi x/\lambda) \end{matrix} \right\} \left\{ \begin{matrix} \exp(\gamma z) \\ \exp(-\gamma z) \end{matrix} \right\} \mathbf{i}_y$$

$$\gamma = \sqrt{(2\pi/\lambda)^2 - j2\pi f \mu\sigma} = \sqrt{(2\pi/\lambda)^2 - 2j/\delta^2}$$

$$\delta = \sqrt{1/\pi f \mu\sigma}$$ (skindepth)

$$\Phi \propto \left\{ \begin{matrix} \cos(2\pi x/\lambda) \\ \sin(2\pi x/\lambda) \end{matrix} \right\} \left\{ \begin{matrix} \exp(\gamma z) \\ \exp(-\gamma z) \end{matrix} \right\}$$

$$\gamma = 2\pi/\lambda$$

In the dielectric case, the depth of sensitivity, $1/\gamma$, does not depend on frequency.

© JENTEK Sensors 2009

Sensor Structure, Periodicity, Wavelength, and Fourier Series

Magnetoquasistatic (MWM)

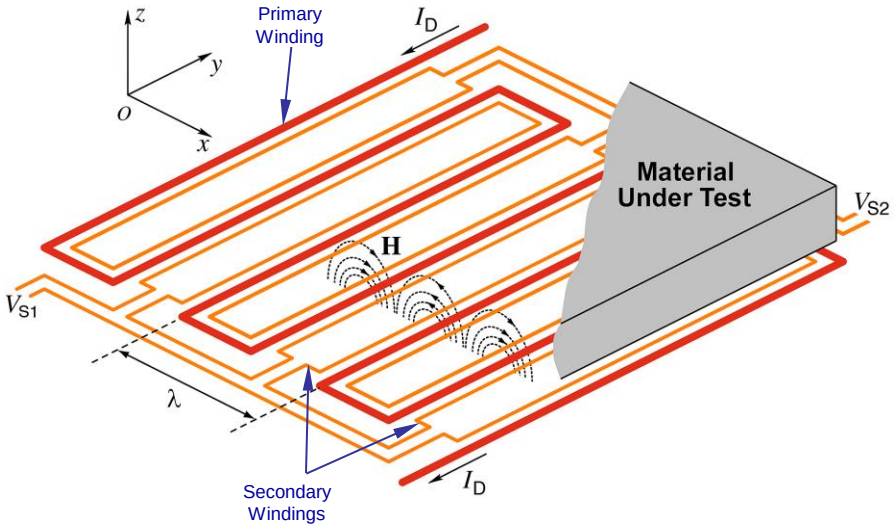

Electroquasistatic (IDED)

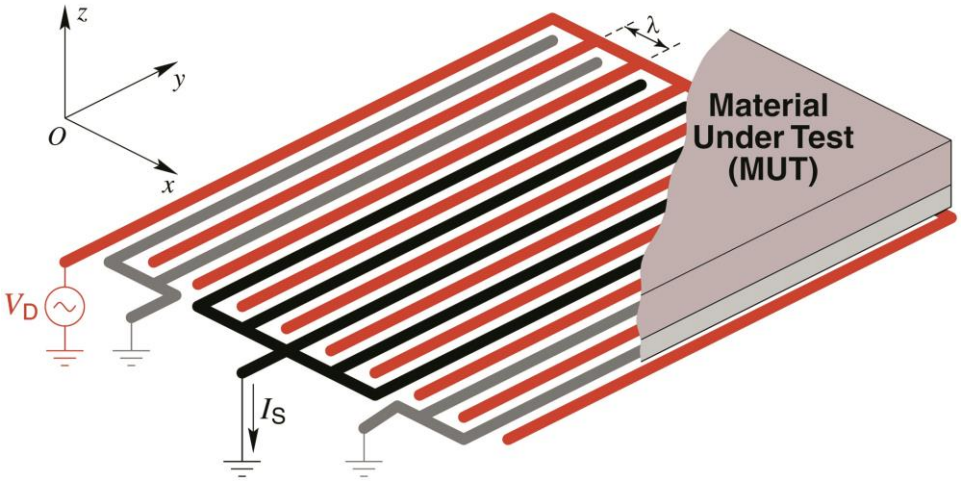

The sensors are designed to fit the assumptions that make it possible to use the simple solutions (periodic, with dummy elements that make them look infinite, etc.).

They are periodic, but ***not*** sinusoidal. Solution: break the solution up into a ***sum*** of sinusoids with wavelengths λ, $\lambda/2$, $\lambda/3$, etc., using ***Fourier Series***, solve for each separately, then put the solution back together at the end.

© JENTEK Sensors 2009

Computing Transimpedance, Surface Reluctance/Capacitance Density

Magnetoquasistatic (MWM)

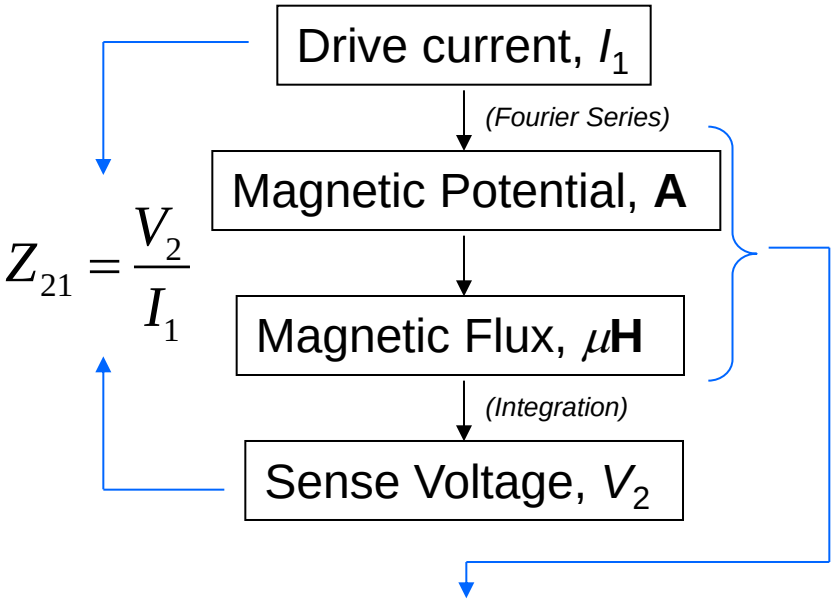

$$H_x = RA_y$$

R contains all the information about the material properties and geometry. At the bottom of an infinitely thick layer,

$$R = \frac{\gamma}{\mu}$$

Electroquasistatic (IDED)

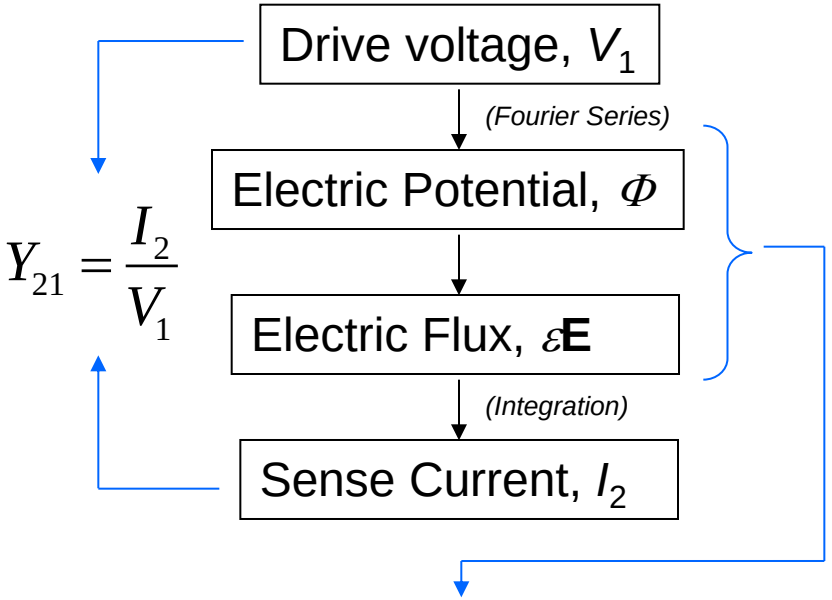

$$\varepsilon E_z = C\Phi$$

C contains all the information about the material properties and geometry. At the bottom of an infinitely thick layer,

$$C = \gamma\varepsilon = \frac{2\pi}{\lambda}\varepsilon$$

© JENTEK Sensors 2009

Matching Boundary Conditions, Multiple Layers, and Transfer Relations

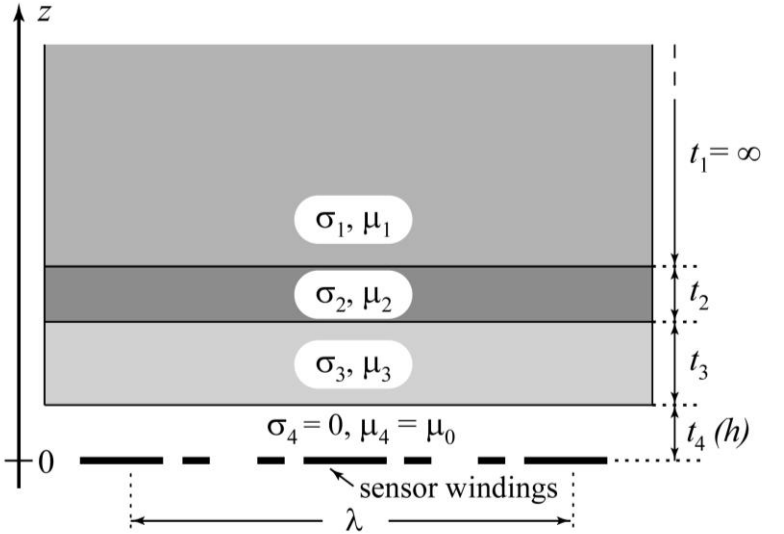

At every layer interface:

- The potential must be continuous
- The flux must be continuous

This lets us match the solutions in every layer. It turns out that if we know R or C at the top of a layer, we can obtain it at the bottom.

$$R_{\text{bottom}} = \frac{\gamma}{\mu} \cdot \frac{\mu R_{\text{top}} \coth(\gamma t) + \gamma}{\mu R_{\text{top}} + \gamma \coth(\gamma t)}$$

$$C_{\text{bottom}} = \gamma\varepsilon \cdot \frac{C_{\text{top}} \coth(\gamma t) + \gamma\varepsilon}{C_{\text{top}} + \gamma\varepsilon \coth(\gamma t)}$$

In this way, all information about all material layers is contained in a single quantity: R or C at the sensor windings or electrodes.

© JENTEK Sensors 2009

Collocation Point Method

Approximates the unknown potential as an interpolation between its values at a set of points, called the **collocation points**. These values are computed by solving a set of simultaneous equations, each of which is derived from a boundary condition applied over a spatial interval that contains the corresponding collocation point.

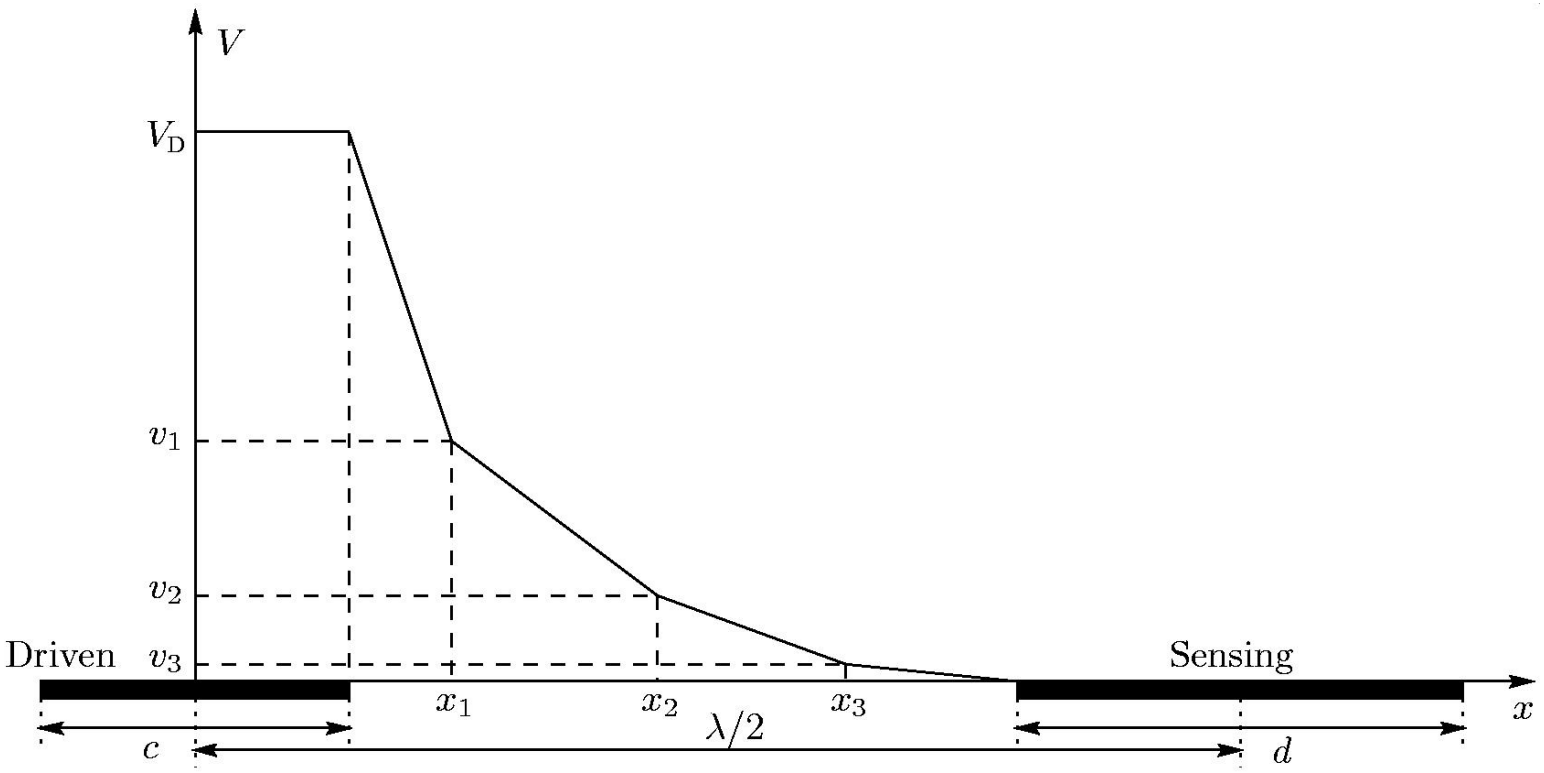

© JENTEK Sensors 2009

Multivariate Inverse Methods

- The Need for Inverse Interpolation
- Approaches to Solving the Inverse Problem
- One-Dimensional Inverse Interpolation
- Two-Dimensional Inverse Interpolation
- Interpolation and Extrapolation Methods
- Overconstrained Problems
- Summary

© JENTEK Sensors 2009

The Need for Inverse Interpolation

Forward problem:

Material Properties: σ, μ, ε
Material Geometry: h, Δ
Sensor Geometry: λ, etc.

⇨ Sensor Model ⇨ Transimpedance for every frequency and element, $Z_{21}(f, e)$

Inverse problem:

Sensor Response: $Z_{21}(f, e)$ ⇨ **?** ⇨ σ, μ, ε, h, Δ , etc.

Correlation with → **Material or process behavior/ parameters of interest**

- If the number of unknowns is equal to the number of "equations" or "knowns" (two for every frequency/element combination), it *might* be possible to find an exact solution.
- In general, we are looking for a set of values for the unknowns that will yield the best match to the measured transimpedances.

In general, it is not possible to solve the inverse problem in "closed form," i.e., derive direct formulas or methods.

© JENTEK Sensors 2009

Approaches to Solving the Inverse Problem

The inverse problem must be solved iteratively:

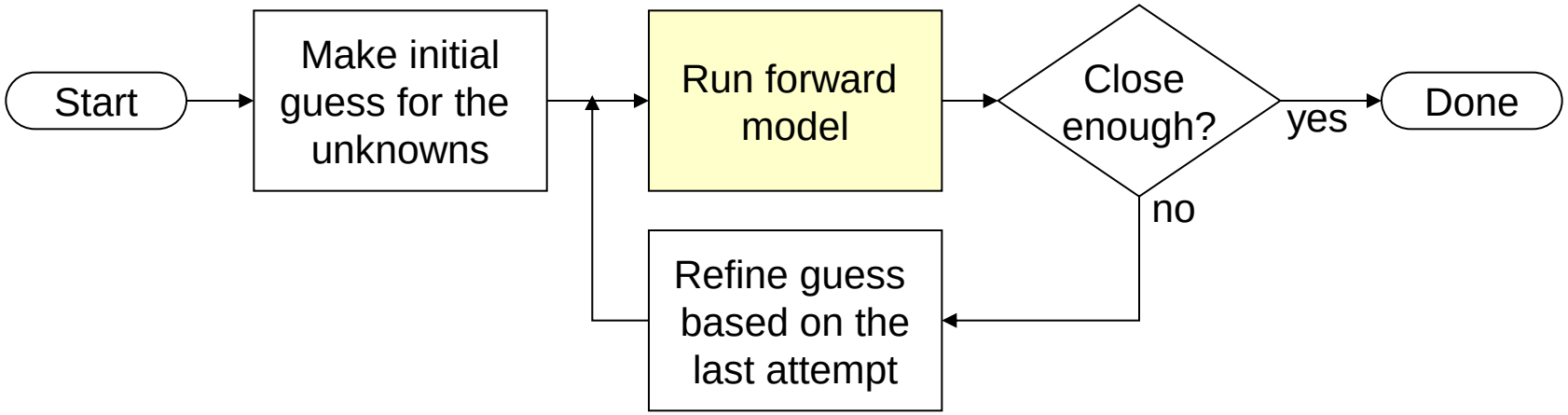

Problems with this approach:

- Requires the client/user to have access to the tools that implement the forward model.
- It is slow, not suited for real-time applications.
- Not guaranteed to converge to a solution even if one exists.
- At the end of the estimation, any knowledge collected along the way is lost.

*Solution: generate (off-line) a database of precomputed sensor responses and then find the answer via **inverse interpolation**.*

© JENTEK Sensors 2009

One-Dimensional Inverse Interpolation

Example: single-wavelength IDED used to measure dielectric permittivity.

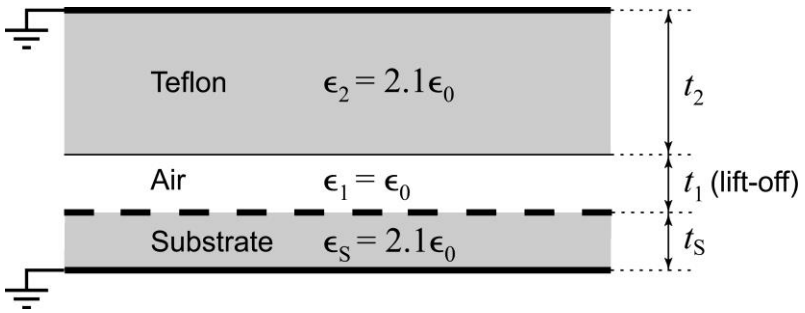

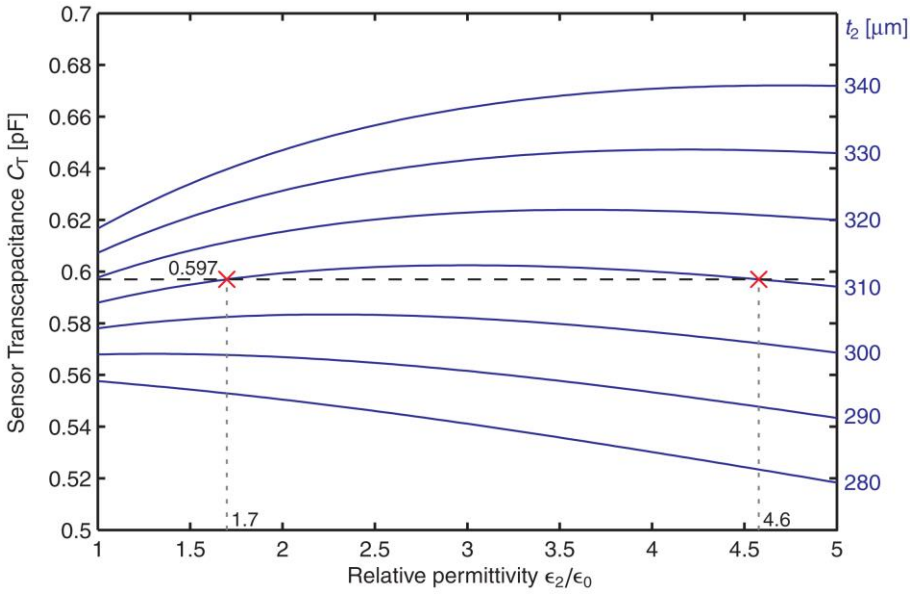

- Forward interpolation (using the curves to get C_T from ε_2) is easy.
- Inverse interpolation (using the curves to get ε_2 from C_T) is hard: there can be one, two, or no solutions.

  …but at least we can see this right away, by traversing the curve and seeing if we encounter the transcapacitance value.

This cannot be done in two or more dimensions!

© JENTEK Sensors 2009

Measurement Grids

- Create a database of responses prior to data acquisition for the range of properties of interest
  - In two-dimensions, can be plotted as a grid

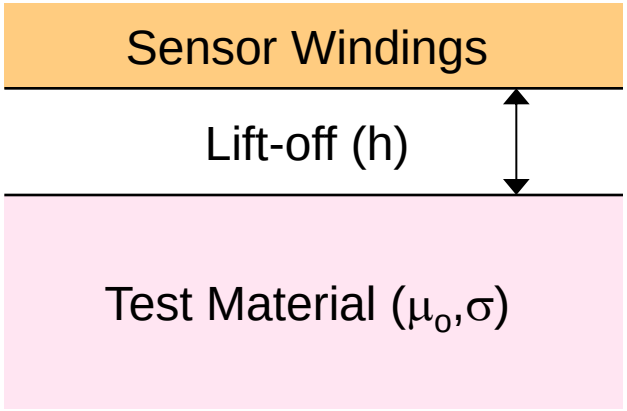

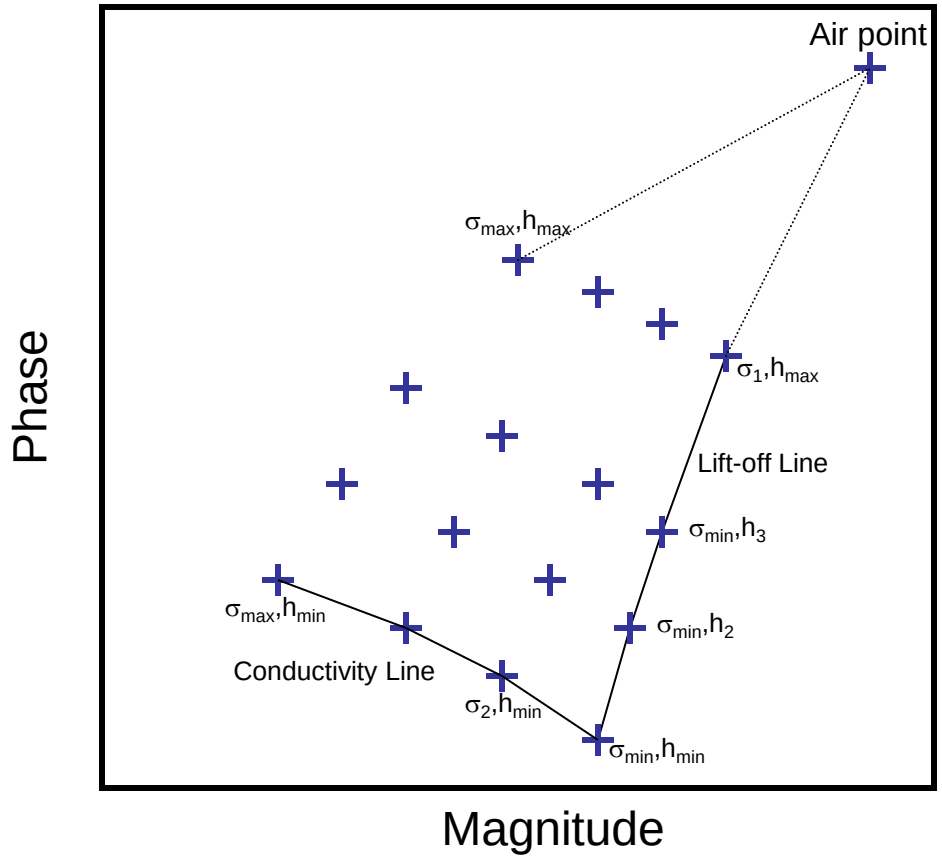

© JENTEK Sensors 2009

Examples of Two-Dimensional Inverse Interpolation Issues

Closest point is not necessarily correct (happens all the time).

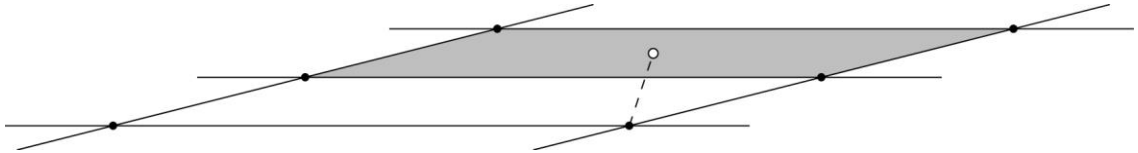

What to do when edges cross (happens all the time).

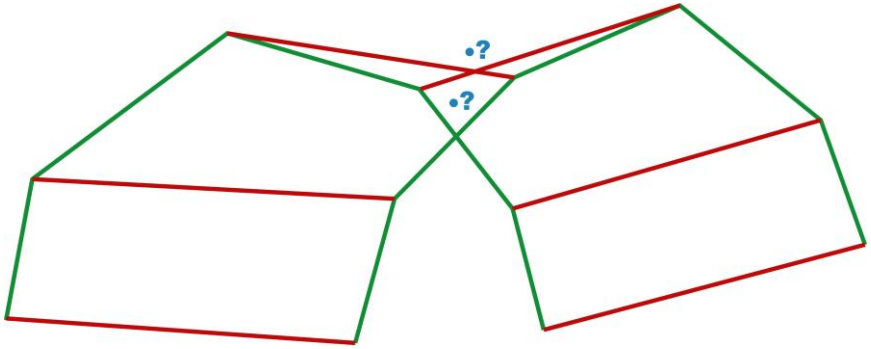

Are we “on the grid”?

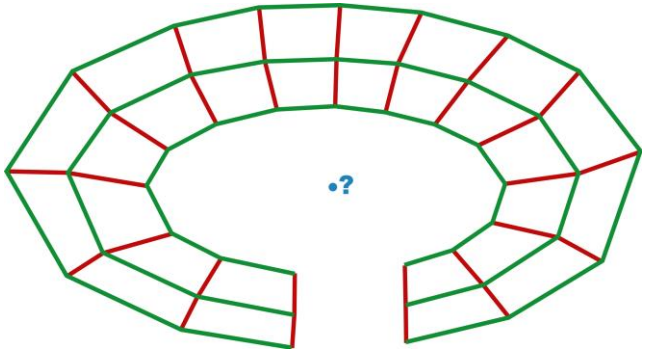

The hardest thing to do is determining whether a point is on the grid and which grid cell to use for interpolation.

© JENTEK Sensors 2009

Overconstrained Problems
(more equations than unknowns)

Every grid cell defines a (hyper) space via the direction vectors associated with each property.

If the target point does not lie in this space, we work with its ***orthogonal projection***.

This is **guaranteed to produce the best solution** in the least squares sense.

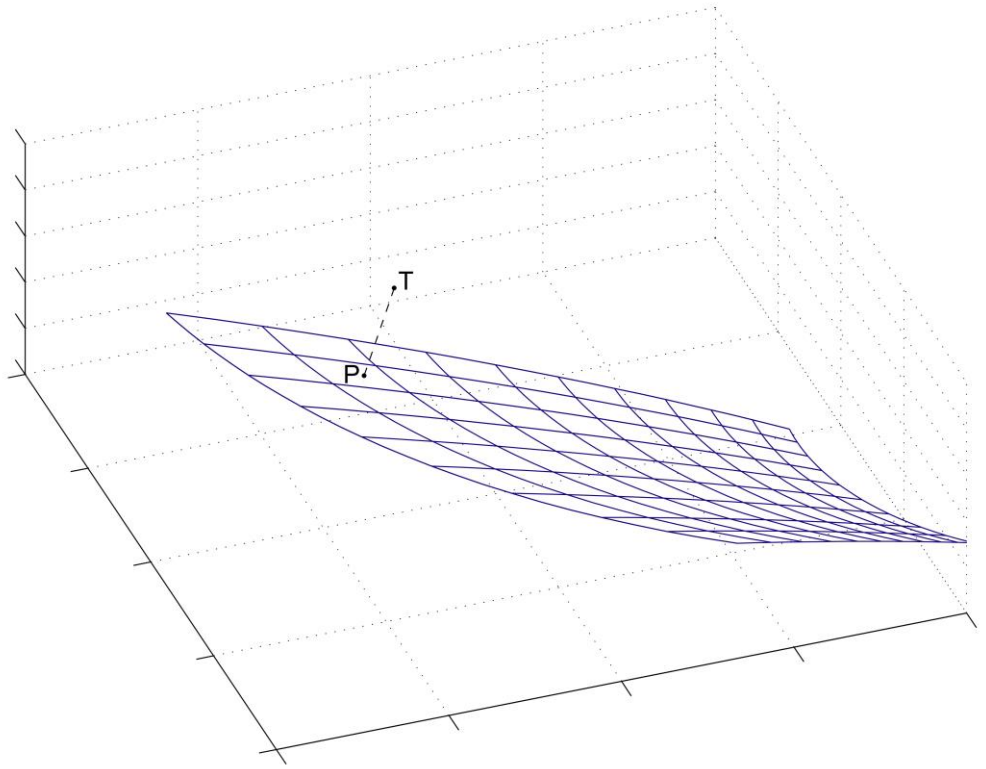

Example: 2-D grid in 3-D impedance space. Point P is the orthogonal projection of point T onto the plane of the particular grid cell

© JENTEK Sensors 2009

Matrix of Partial Derivatives, Pseudoinverse, and Singular Value Decomposition

Let $k_1 \ldots k_n$ be the unknowns and $z_1 \ldots z_m$ be the impedance measurements (i.e., "equations"). The Jacobian matrix defines the directions in impedance space in which each of the unknown properties change. $m \geq n$

$$\Delta \mathbf{z} = \mathbf{M} \cdot \Delta \mathbf{k}$$

$$\mathbf{M} = \begin{bmatrix} \frac{\partial z_1}{\partial k_1} & \frac{\partial z_1}{\partial k_2} & \cdots & \frac{\partial z_1}{\partial k_n} \\ \frac{\partial z_2}{\partial k_1} & \frac{\partial z_2}{\partial k_2} & \cdots & \frac{\partial z_2}{\partial k_n} \\ \vdots & \vdots & \ddots & \vdots \\ \vdots & \vdots & \ddots & \vdots \\ \frac{\partial z_m}{\partial k_1} & \frac{\partial z_m}{\partial k_2} & \cdots & \frac{\partial z_m}{\partial k_n} \end{bmatrix}$$

Direction vector of increasing k_2

where $\Delta \mathbf{z}$ is the vector connecting the reference point (origin) to the target point and $\Delta \mathbf{k}$ are the property estimate offsets from the property values at the reference point.

If **P** is the ***pseudoinverse*** matrix of **M** then

$$\Delta \mathbf{k} = \mathbf{P} \cdot \Delta \mathbf{z} \qquad \mathbf{P} = \left(\mathbf{M}^{\mathrm{T}}\mathbf{M}\right)^{-1}\mathbf{M}^{\mathrm{T}}$$

The pseudoinverse **P** is computed via ***Singular Value Decomposition***. If any of the singular values are zero (or very small) then the matrix **M** is singular and the ***selectivity*** at this grid point is low, i.e., the unknown properties are not independent.

$$\mathbf{M} = \mathbf{U}\mathbf{W}\mathbf{V}^{\mathrm{T}} \quad \rightarrow \quad \mathbf{P} = \mathbf{V}\mathbf{W}^{-1}\mathbf{U}^{\mathrm{T}}$$

© JENTEK Sensors 2009

Selected References

Goldfine, N., "Uncalibrated, Absolute Property Estimation and Measurement Optimization for Conducting and Magnetic Media Using Imposed w-k Magnetometry," Ph.D. thesis, Massachusetts Institute of Technology, September, 1990.

Goldfine, N.; *"*Magnetometers for Improved Materials Characterization in Aerospace Applications,*"* *Materials Evaluation*, Vol. 51, No. 3; pp. 396-405, March 1993.

Goldfine, N., Zilberstein, V., Cargill, S., Schlicker, D., Shay, I., Washabaugh, A., Tsukernik, V., Grundy, D., Windoloski, M., "MWM-Array Eddy Current Sensors for Detection of Cracks in Regions with Fretting Damage," *Materials Evaluation*, Vol. 60, No. 7, pp 870-877; July 2002.

Goldfine, N., Sheiretov, Y., Schlicker, D., Washabaugh, A., "Rapid, Nonlinear "System" Identification for NDT, Using Sensor Response Databases," *Materials Evaluation*, Vol. 66, No. 7, July 2008, pp747-755.

Goldfine, N. Washabaugh, A., Sheiretov, Y., Windoloski, M. (2009). Eddy-current Methods, in *Encyclopedia of Structural Health Monitoring*, Boller, C., Chang, F. and Fujino, Y. (eds). John Wiley & Sons Ltd, Chichester, UK, pp 393-412.

Goldfine, N.., Lovett, T., Sheiretov, Y., Zombo, P. "Dielectrometers and Magnetometers, Suitable for In-situ Inspection of Ceramic and Metallic Coated Components," SPIE proceedings, Vol. 2459, pp. 164-174, 1995.

Melcher, J.; *"Continuum Electromechanics,"* MIT Press, 1981.

Haus, H. and **Melcher, J.**; "*Electromagnetic Fields and Energy*," Prentice-Hall, 1989.

Schlicker, D., "Imaging of Absolute Electrical Properties Using Electroquasistatic and Magnetoquasistatic Sensor Arrays," Ph.D. thesis, Dept. of Electrical Engineering and Computer Science, Massachusetts Institute of Technology, Cambridge, MA, June 2006.

Sheiretov, Y., "Deep Penetration Magnetoquasistatic Sensors," Ph.D. thesis, Massachusetts Institute of Technology, June, 2001.

Sheiretov, **Y.** "Dielectrometry Measurements of Moisture Dynamics in Oil-Impregnated Pressboard," M.S. thesis, Dept. of Electrical Engineering and Computer Science, Massachusetts Institute of Technology, Cambridge, MA, May 1994.

Sheiretov, **Y.,** "Deep Penetration Magnetoquasistatic Sensors," Ph.D. thesis, Dept. of Electrical Engineering and Computer Science, Massachusetts Institute of Technology, June, 2001, pp. 48-59, 69-75.

Washabaugh, A., "Flow induced electrification of liquid insulated systems," Sc.D thesis, Dept. of Electrical Engineering, Massachusetts Institute of Technology, Cambridge, MA, 1995.

Washabaugh, A., Sheiretov, Y., Schlicker, D. E., Goldfine, N. J., "Non-Contact Capacitive Sensing Dielectrometers for Characterization of Adhesives and Epoxies," ASNT Fall Conference 2000, Indianapolis, IN, November 2000.

© JENTEK Sensors 2009

Questions?

For more information, contact us via email:
jentek@shore.net

© JENTEK Sensors 2009